



ENDOMETRIOSIS

Fusobacterium infection facilitates the development of endometriosis through the phenotypic transition of endometrial fibroblasts

Ayako Muraoka^{1,2}, Miho Suzuki¹, Tomonari Hamaguchi³, Shinya Watanabe¹, Kenta Iijima¹, Yoshiteru Murofushi¹, Keiko Shinjo¹, Satoko Osuka², Yumi Hariyama⁴, Mikako Ito³, Kinji Ohno³, Tohru Kiyono⁵, Satoru Kyo⁶, Akira Iwase⁷, Fumitaka Kikkawa², Hiroaki Kajiyama², Yutaka Kondo^{1,8,*}

Copyright © 2023 The Authors, some rights reserved; exclusive licensee American Association for the Advancement of Science. No claim to original U.S. Government Works

Retrograde menstruation is a widely accepted cause of endometriosis. However, not all women who experience retrograde menstruation develop endometriosis, and the mechanisms underlying these observations are not yet understood. Here, we demonstrated a pathogenic role of *Fusobacterium* in the formation of ovarian endometriosis. In a cohort of women, 64% of patients with endometriosis but <10% of controls were found to have *Fusobacterium* infiltration in the endometrium. Immunohistochemical and biochemical analyses revealed that activated transforming growth factor- β (TGF- β) signaling resulting from *Fusobacterium* infection of endometrial cells led to the transition from quiescent fibroblasts to transgelin (TAGLN)-positive myofibroblasts, which gained the ability to proliferate, adhere, and migrate in vitro. *Fusobacterium* inoculation in a syngeneic mouse model of endometriosis resulted in a marked increase in TAGLN-positive myofibroblasts and increased number and weight of endometriotic lesions. Furthermore, antibiotic treatment largely prevented establishment of endometriosis and reduced the number and weight of established endometriotic lesions in the mouse model. Our data support a mechanism for the pathogenesis of endometriosis via *Fusobacterium* infection and suggest that eradication of this bacterium could be an approach to treat endometriosis.

INTRODUCTION

Endometriosis is caused by endometrial-like tissue containing endometrial glands and extensive fibrotic tissue growing outside the endometrial cavity, most often in the pelvic peritoneum or ovaries, resulting in chronic pelvic pain and infertility (1). It is a common gynecological disease affecting 10 to 15% of women of reproductive age (2). Several hypotheses have been proposed to explain the cause of endometriosis, including retrograde menstruation, coelomic metaplasia, and the presence of Mullerian remnants (3). Of these, retrograde menstruation, where menstrual blood flows back through the fallopian tubes and into the pelvic cavity instead of out of the vagina, is widely accepted as a cause of endometriosis. However, although most women of reproductive age experience retrograde menstruation (3), only 10 to 15% of women develop endometriosis. This suggests the existence of other mechanisms that facilitate the development of endometriosis.

Although endometriosis outgrowths are benign, the abundant desmoplastic stroma, where robust fibroblast proliferation and migration are promoted by secreted growth factors, is clinically problematic (4). The characteristics of the stromal fibroblasts are key determinants of the growth of newly established endometriosis and subsequently its progression (5). Recent studies have revealed that quiescent fibroblasts are activated to differentiate into myofibroblasts during wound healing and chronic inflammatory conditions such as fibrosis and cancer (6–8). Activated myofibroblasts contain cytoplasmic microfilament-associated proteins such as α -smooth muscle actin (α SMA; encoded by *ACTA2*), vimentin (VIM), and transgelin [TAGLN; also known as smooth muscle 22 α (SM22 α)]. The latter is a calponin-related actin-binding cytoskeletal protein that is linked to increased cell motility and migration and is expressed in mesenchymal lineage cell types (myofibroblasts and smooth muscle cells) (9, 10). The transition from quiescent fibroblasts to activated myofibroblasts is triggered by chronic inflammation that involves the production of multiple cytokines, including transforming growth factor- β (TGF- β) (6, 11, 12).

Although a large proportion of the bacteria in the vagina are Lactobacilli, studies have documented the presence of other types of bacteria as well, such as *Fusobacterium nucleatum*, which may be associated with vaginal dysbiosis in certain situations (13, 14). Species of the *Fusobacterium* genus are known to be common members of the oral and gastrointestinal tract microbiota and have a symbiotic relationship with its hosts (15). Although the uterine cavity is believed to be almost sterile, a close association between endometriosis and endometritis has been reported (16). Recent highly sensitive 16S ribosomal RNA (rRNA) gene amplicon

¹Division of Cancer Biology, Nagoya University Graduate School of Medicine, 65 Tsurumai-cho, Showa-ku, Nagoya 466-8550, Japan. ²Department of Obstetrics and Gynecology, Nagoya University Graduate School of Medicine, 65 Tsurumai-cho, Showa-ku, Nagoya 466-8550, Japan. ³Division of Neurogenetics, Nagoya University Graduate School of Medicine, 65 Tsurumai-cho, Showa-ku, Nagoya 466-8550, Japan. ⁴Department of Obstetrics and Gynecology, Toyota Kosei Hospital, 500-1, Itohara, Ziyosui-cho, Toyota 470-0396, Japan. ⁵Project for Prevention of HPV-related Cancer, Exploratory Oncology Research and Clinical Trial Center, National Cancer Center, Kashiwanoha 6-5-1, Kashiwa 277-8577, Japan. ⁶Department of Obstetrics and Gynecology, Shimane University Faculty of Medicine, 89-1 Enya-cho, Izumo 693-8501, Japan. ⁷Department of Obstetrics and Gynecology, Gunma University Graduate School of Medicine, 3-39-22 Showa-machi, Maebashi 371-8511, Japan. ⁸Institute for Glyco-core Research (iGCORE), Nagoya University, Furo-cho, Chikusa-ku, Nagoya 464-8601, Japan.

*Corresponding author: Email: ykondo@med.nagoya-u.ac.jp

sequencing has demonstrated that, although the amount of bacteria in the uterus is about four orders of magnitude less than in the vagina, certain microbial communities, including members of the *Fusobacterium* genus, can be detected (17). Although members of the *Fusobacterium* genus have long been considered opportunistic pathogens, recent studies revealed that some *Fusobacterium* species such as *F. nucleatum* play an important role not only in periodontitis but also in carcinogenesis via induction of several inflammatory cytokines, such as interleukin-6 (IL-6), IL-8, and tumor necrosis factor (TNF) (15). In this study, we asked whether the endometrial stromata of patients with endometriosis contained different types of fibroblasts compared with people without endometriosis and whether these fibroblasts might be associated with the presence of specific pathogenic bacteria.

RESULTS

TAGLN is up-regulated in fibroblasts from patients with endometriosis

First, we undertook gene expression profiling and compared uterus endometrial fibroblasts from patients without endometriosis (UTnon-FBs; $n = 4$, two in menstrual cycle proliferative phase and two in secretory phase) with those from ovarian endometriotic lesions [ovarian endometriotic fibroblasts (OVend-FBs); $n = 4$, also two in each phase]. There was no significant difference in age, menstrual period, gravidity and parity, or history of repeated surgery between patients with UTnon-FBs and OVend-FBs ($P > 0.05$, Fisher's exact test; tables S1 to S3). We found that 1187 genes were significantly up-regulated and 1084 down-regulated in endometriotic tissues [defined as fold change (FC) > 2.0 , $P < 0.05$; Fig. 1, A and B, and fig. S1A]. The expression profiles in our dataset were compared with three public datasets of normal human endometrium and endometriosis samples (GSE25628, GSE99949, and GSE7305), which were derived from endometrial or endometriosis tissue (18–20). This revealed that 10 genes were up-regulated and 3 were down-regulated in endometriosis samples relative to normal endometrial tissues across all four datasets (table S4).

The expression of these 13 genes was validated by quantitative reverse transcription polymerase chain reaction (qRT-PCR) in primary UTnon-FBs ($n = 14$) compared with primary OVend-FBs and primary fibroblasts from the corresponding eutopic endometrial tissues [uterus endometrial fibroblasts with endometriosis (UTend-FBs)] from patients with endometriosis ($n = 14$). Of these 13 genes, there was a significant stepwise increasing mRNA expression for only *TAGLN*, with the lowest amount in UTnon-FBs, followed by UTend-FBs and OVend-FBs ($P < 0.05$ and $P < 0.01$ for UTnon-FBs versus UTend-FBs and UTend-FBs versus OVend-FBs, respectively; Fig. 1C and fig. S1, B to D). *TAGLN* protein amounts were also increasingly up-regulated in UTnon-FBs and UTend-FBs, and the greatest abundance was found in OVend-FBs ($P < 0.01$; Fig. 1D). Fibroblasts in only a part of the endometrium expressed *TAGLN*, but this protein was present in most fibroblasts in the corresponding ovarian endometriotic lesions from the same patients with endometriosis (Fig. 1E and fig. S1F).

Gene expression profiling was further examined by single-cell RNA sequencing (scRNA-seq). In the endometrium without endometriosis (UTnon-EM) and ovarian endometriosis (OVend) samples, scRNA-seq revealed that cells classified into groups, including epithelial cells, macrophages/monocytes, mast cells, T

cells/natural killer (NK) cells, endothelial cells, or fibroblasts, expressed characteristic marker genes for each type of cell (fig. S2, A to C) (21). Fibroblasts from UTnon-EM and OVend were classified into distinct subpopulations (Fig. 1F). *TAGLN* was substantially up-regulated in the subpopulation of fibroblasts from OVend (Fig. 1, F and G). Nine of 10 genes identified as up-regulated by gene expression profiling were more highly expressed in fibroblasts from OVend than from UTnon-EM (table S5).

Up-regulation of TAGLN promotes fibroblast proliferation and mobility

TAGLN functions as an actin cross-linking protein of the calponin family and is a marker of myofibroblasts (9, 10). It is localized to the cytoskeletal apparatus and confers contractile function on cells (22). The established OVend-FB cell lines SC8 and SC10 retained higher expression of *TAGLN* mRNA and protein than the UTnon-FB cell lines MC1 and MC2 (Figs. 1A and 2, A and B). Characteristic expression profiles of myofibroblast markers, such as *ACTA2*, *TAGLN*, platelet-derived growth factor subunit A (*PDGFA*), and *VIM*, in these four cell lines revealed that SC8 and SC10 represented myofibroblasts, whereas MC1 and MC2 represented quiescent fibroblasts (fig. S3, A to D) (6).

Depletion of *TAGLN* by small interfering RNA (siRNA) transfection significantly decreased proliferation of OVend-FB cell lines SC8 and SC10 ($P < 0.05$; Fig. 2C and fig. S4, A and B). *TAGLN* depletion also impaired the migration ability of OVend-FB cell lines and their attachment to mesothelial cells (Fig. 2, D and E). Reciprocally, overexpression of *TAGLN* by transfection of a *TAGLN*-expressing vector in the UTnon-FB cell lines MC1 and MC2 increased proliferation, migration, and attachment (fig. S4, C to G).

TAGLN-expressing OVend-FBs promote endometrial cell proliferation via IL-6

Colocalization of *TAGLN* with circular bundles of actin (α SMA) microfilaments was observed in OVend-FBs that had a polygonal shape (Fig. 2F). The abundance of both *TAGLN* and α SMA was increased in cell lines SC8 and SC10 (Fig. 2B and fig. S5A). Depletion of *TAGLN* by siRNA transfection in cell lines SC8 and SC10 resulted in marked morphological changes, with cells taking an elongated spindle shape in which circular actin bundles were no longer present and straight bundles were formed across the cell body, with no change of α SMA expression (Fig. 2F and fig. S5B). These morphological changes suggest that the cells may have decreased contractility. The cell lines MC1 and MC2 overexpressing *TAGLN* obtained a polygonal shape (fig. S5C).

The C-terminal calponin-like module (CLIK) of *TAGLN* (Fig. 2G) is known to interact with α SMA, which confers contractility to cells (23). Overexpression of *TAGLN*- Δ CLIK in *TAGLN*-depleted SC8 and SC10 cells using si-TAGLN#2 (see Materials and Methods) altered the colocalization of *TAGLN* and α SMA. *TAGLN* accumulated at the centers of the cells, resulting in an enlarged, flattened shape (Fig. 2H). Transfection of *TAGLN*-FL (full-length *TAGLN*) into the MC2 cell line resulted in the acquisition of a polygonal shape, whereas *TAGLN*- Δ CLIK took on an enlarged, flattened shape (fig. S5D).

Myofibroblasts produce and secrete a number of cytokines when they contract (24). We examined cytokines correlating with *TAGLN* expression in cell lines of UTnon-FBs or OVend-FBs and found that IL-6 was the most prominent among the 30 cytokines and growth

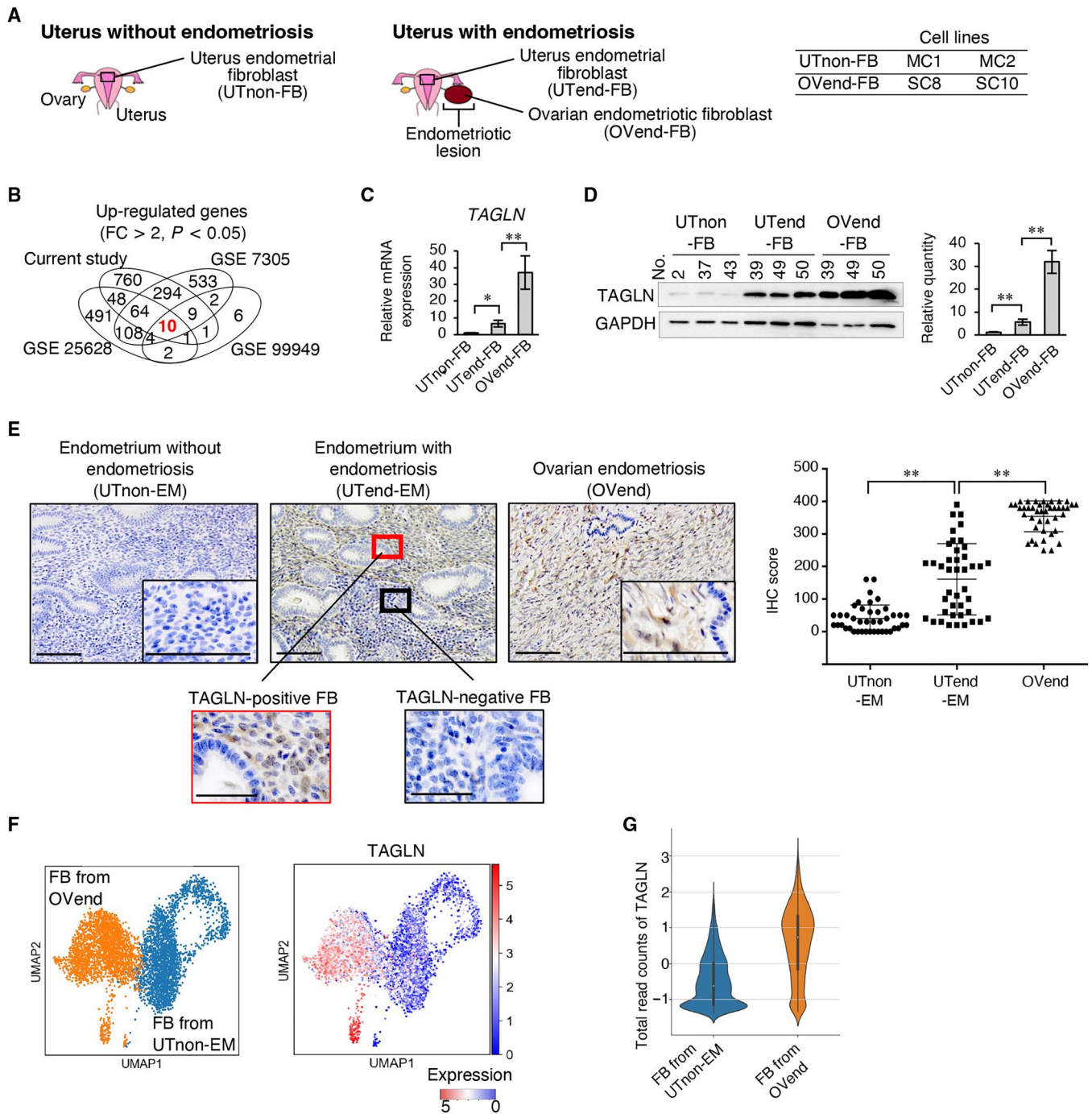


Fig. 1. Up-regulation of TAGLN in both eutopic endometrial and ovarian endometriotic fibroblasts from patients with endometriosis. (A) Schema of fibroblasts and immortalized cell lines in this study. (B) Venn diagram of up-regulated genes in OVend-FBs combined with the public data. (C) mRNA expression of *TAGLN* in primary UTnon-FBs ($n = 14$), UTend-FBs ($n = 14$), and OVend-FBs ($n = 14$). The y axis indicates the mRNA of *TAGLN* relative to glyceraldehyde-3-phosphate dehydrogenase (*GAPDH*). (D) *TAGLN* protein abundance in primary fibroblasts from each patient (in the left gel image, patient numbers correspond to table S1). The expression of *TAGLN* relative to *GAPDH* was calculated (right, $n = 3$ in each group). (E) Immunohistochemistry of *TAGLN* in endometrium without endometriosis (UTnon-EM), endometrium with endometriosis (UTend-EM), and ovarian endometriosis (OVend) (left). IHC scores of UTnon-EM ($n = 42$), UTend-EM ($n = 42$), and OVend ($n = 42$) are shown as dot plots (right). (F) UMAP plots of *TAGLN* expression within the fibroblast subpopulation (right). Orange- and turquoise-colored fibroblast cells were derived from OVend and UTnon-EM, respectively (left). (G) Violin plots of total read count of *TAGLN* within fibroblasts. Scale bars, 100 μm . Error bars indicate SEM (C and D) or SD (E). * $P < 0.05$ and ** $P < 0.01$. Data were analyzed by two-tailed Student's *t* test.

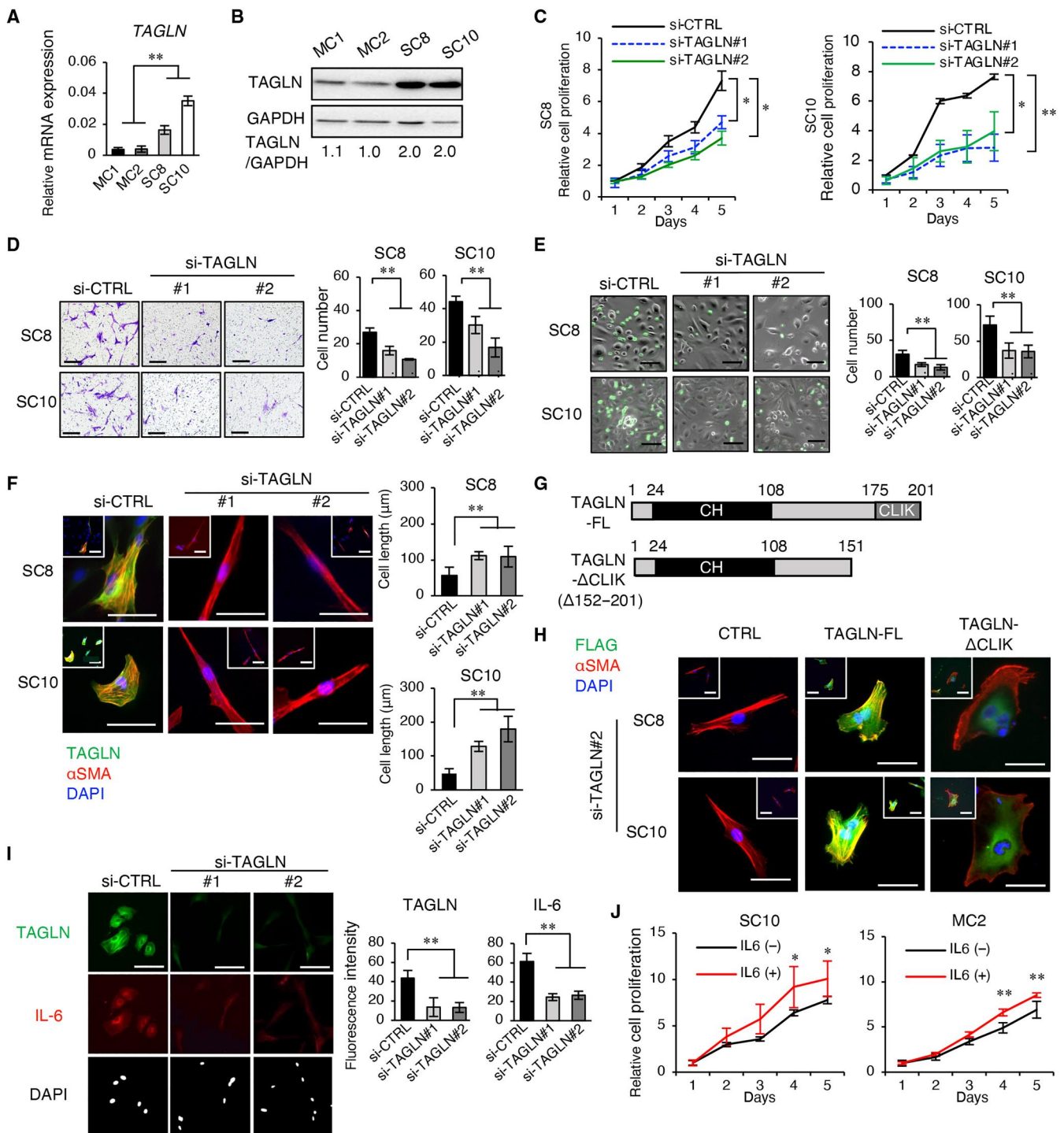


Fig. 2. Functional analyses of TAGLN in endometrial and endometriotic fibroblasts. (A and B) TAGLN mRNA (A) and protein (B) in the MC1, MC2, SC8, and SC10 cell lines. The y axis indicates the mRNA of TAGLN relative to GAPDH (A). Ratios of TAGLN to GAPDH are shown below the gel images (B). (C to E) Cell proliferation (C), migration (D), and attachment assays (E) of the SC8 and SC10 cell lines after TAGLN depletion. The y axis indicates cell proliferation rate relative to day 1 (C). The bar graphs show the number of migrated or expressing GFP-attached cells (D and E). Scale bars, 100 μm. (F) Presence of TAGLN (green) and αSMA (red, left) and quantification of cell length (right) in SC8 and SC10 cells with siRNA against TAGLN (#1, #2). For each sample, 30 cells were measured. Nuclei were stained with DAPI (blue). Insets, lower magnifications. Scale bars, 50 μm. (G) Schema of full-length (FL) and truncated (ΔCLIK 152 to 201) TAGLN protein. CH, calponin homology; CLIK, C-terminal calponin-like module. (H) Localization of exogenous Flag-tagged TAGLN. Scale bars, 50 μm. (I) Presence of TAGLN (green) and IL-6 (red) in SC10 after depletion of TAGLN (left). Mean fluorescence intensity of each cell was quantified (right). Thirty cells were analyzed per sample. Nuclei were stained with DAPI. Scale bars, 100 μm. (J) Proliferation of MC2 and SC10 cells with/without IL-6 treatment (10 ng/ml). The y axis indicates cell proliferation rate relative to day 1. Error bars indicate SD (A, C to F, I, and J). **P* < 0.05 and ****P* < 0.01. Data were analyzed by one-way ANOVA (A, D to F, and I) or two-tailed Student's *t* test (C and J), respectively.

factors tested on the protein array (Fig. 2I and fig. S6A). However, overexpression of TAGLN- Δ CLIK did not up-regulate IL-6 production (fig. S6B) (25). Addition of recombinant IL-6 to the cell culture medium promoted the proliferation of all four cell lines tested (Fig. 2J and fig. S6C). Consistent with this *in vitro* analysis, clinical samples also expressed IL-6 at increasing amounts in endometria from patients without endometriosis ($n = 10$), more in endometria ($n = 10$), and most in the corresponding ovarian endometriotic lesions from patients with endometriosis ($n = 16$) (fig. S6D). Furthermore, the protein expression of TAGLN was positively correlated with IL-6 in these tissues (fig. S6E).

TGF- β 1 induces the expression of TAGLN

TGF- β 1 is known to be a key growth factor that plays a major role in endometriosis (26, 27). Furthermore, TGF- β 1 is known to induce myofibroblast-associated genes (fig. S7A), including TAGLN, via sma- and mad-related (SMAD) binding to its promoter (28). We therefore asked whether TGF- β signaling induced TAGLN expression in the endometrium. Abundance of TGF- β 1 and TGF- β receptor 1 (TGF- β R1) was increased in both stromal cells and epithelial cells in endometrial tissues and endometriotic lesions from patients relative to normal endometrium (Fig. 3, A and B). Treatment with TGF- β 1 increased the abundance of TAGLN in MC1 and MC2 cell lines. Up-regulation of TAGLN after TGF- β treatment was abolished by SB431542, a specific inhibitor of SMAD2/3-mediated signal transduction (Fig. 3C) (29). These changes in protein expression were associated with the enrichment of histone H3 lysine 27 acetylation (H3K27ac) in the enhancer regions and SMAD2/3 in the promoter regions of the TAGLN gene in MC1 and MC2 cell lines (Fig. 3D and fig. S7B). These findings suggested that epigenetic regulation was involved in the transition from quiescent fibroblasts into myofibroblasts via TGF- β signaling.

Fusobacterium infection influences the endometrial microenvironment

We hypothesized that TGF- β abundance in the endometrial microenvironment might be associated with bacterial infection. We analyzed the publicly available dataset from a previous study (PRJEB16013 and PRJEB21098; <https://ebi.ac.uk/ena/browser/home>) (17), which revealed that five bacterial genera were significantly increased in the endometria of patients with endometriosis relative to healthy controls ($P < 0.01$) (table S6, see also Materials and Methods). Among these bacterial genera, the top-ranked species, *Erysipelothrix*, was not present in substantial amounts in endometrial tissues from individuals either with or without endometriosis, as assessed by qPCR analysis (fig. S8A). Therefore, we examined the second-ranking bacterium, *Fusobacterium*. This genus, known as a symbiont organism, was detected by qPCR in our clinical cohort of endometrial tissues (fig. S8A).

Among *Fusobacterium* species, the presence of *F. nucleatum* in the vagina has previously been reported (13). We tested this using the fluorescence in situ hybridization (FISH) probe EUB338, which, based on publicly available bacterial 16S rRNA sequences, covers most of the eubacteria (30), and probes for *Fusobacterium* species (FUSO) (31) or for *F. nucleatum* (FUS664) (32–34). We found significantly higher frequencies of *Fusobacterium* inside endometrial tissues (27 of 42, 64.3%) and endometriotic tissues (22 of 42, 52.4%) from patients with endometriosis than in controls without endometriosis (3 of 42, 7.1%) ($P < 0.01$; Fig. 4, A and B, and fig.

S8B). The amount of infiltrated *Fusobacterium* was significantly higher in both tissues from patients with endometriosis than controls ($P < 0.01$; Fig. 4B). It was notable that the EUB338, FUSO, and FUS664 signals were almost completely colocalized (>96% of the signals were merged), suggesting that the bacteria infiltrating the endometrium were mainly *F. nucleatum* (fig. S8C).

Infiltration of *F. nucleatum* may induce innate immune responses via its membrane lipopolysaccharide (35), and macrophages are the most abundant immune cells within endometriotic lesions (36). We observed increased numbers of macrophages infiltrating endometrial tissues, with a further increase in staining in ovarian endometriotic tissues compared with controls (fig. S9A). Increased numbers of CD163-positive M2 macrophages, which are known to produce TGF- β 1 (37), were present in both of these tissues from patients with endometriosis (Fig. 4, C and D). Immunohistochemistry (IHC) analysis revealed that TGF- β 1 in the stroma was significantly different between *Fusobacterium*-positive and *Fusobacterium*-negative tissues from both UTend-EM (endometrium with endometriosis) and OVend ($P < 0.01$ and $P < 0.05$, respectively; fig. S9B). In contrast, TGF- β 1 in the epithelium was not different between *Fusobacterium*-positive and *Fusobacterium*-negative tissues, although TGF- β 1 is also known to be secreted from epithelial cells ($P > 0.05$; fig. S9B).

We cocultured cells from the macrophage cell line THP1 [THP1-derived macrophages (dTHP1)] with *F. nucleatum* or *Lactobacillus iners*, which are the major indigenous bacteria of the vaginal microbiota in reproductive-age women, especially in Asian countries (38, 39). This revealed that even heat-killed *F. nucleatum* promoted differentiation of dTHP1 cells into M2 macrophages and stimulated the production of TGF- β 1. In contrast, *L. iners* did not do so ($P < 0.05$; Fig. 4E). Furthermore, cell-free supernatants from the cocultures of dTHP1 with *F. nucleatum* increased TAGLN protein expression in MC2 cells ($P < 0.05$; Fig. 4F and fig. S9C). The amounts of *Fusobacterium*, numbers of CD163-positive macrophages, and IHC scores of TGF- β 1 were positively correlated with each other in the endometrial stromal tissues (Fig. 4G). Amounts of *Fusobacterium* and TAGLN expression were significantly correlated in both the endometrial tissues and endometriotic tissues from patients with endometriosis ($P < 0.01$ and $P < 0.01$, respectively), whereas the abundances of both *Fusobacterium* and TAGLN were low in controls (fig. S9D and table S7). Together, these data suggest that *F. nucleatum* within the endometrium may influence TAGLN abundance in fibroblasts via up-regulated TGF- β 1 signaling.

F. nucleatum infection promotes endometriosis in vivo

Next, we asked whether bacterial infection promoted endometriosis in a syngeneic mouse model in which *F. nucleatum* were intravaginally introduced into the uteri of donor BALB/c mice (Fig. 5A). Endometriotic lesions in these models were induced by peritoneal injection of minced endometrial tissue by transferring endometrial tissues from one animal to a syngeneic animal with an intact immune system (40). Stromal cells in endometrial tissues were validated to express both estrogen receptor α (ER α) and β (ER β) (fig. S10A). First, we determined the volume of transferred endometrial tissues from donor mice. Transferring of 1 or 2 mg of tissues from *F. nucleatum*-infected uteri of donor mice resulted in the formation of multiple endometriotic lesions, whereas tissues from *F. nucleatum*-uninfected uteri did not do so, even when stimulated by estrogen (Fig. 5B).

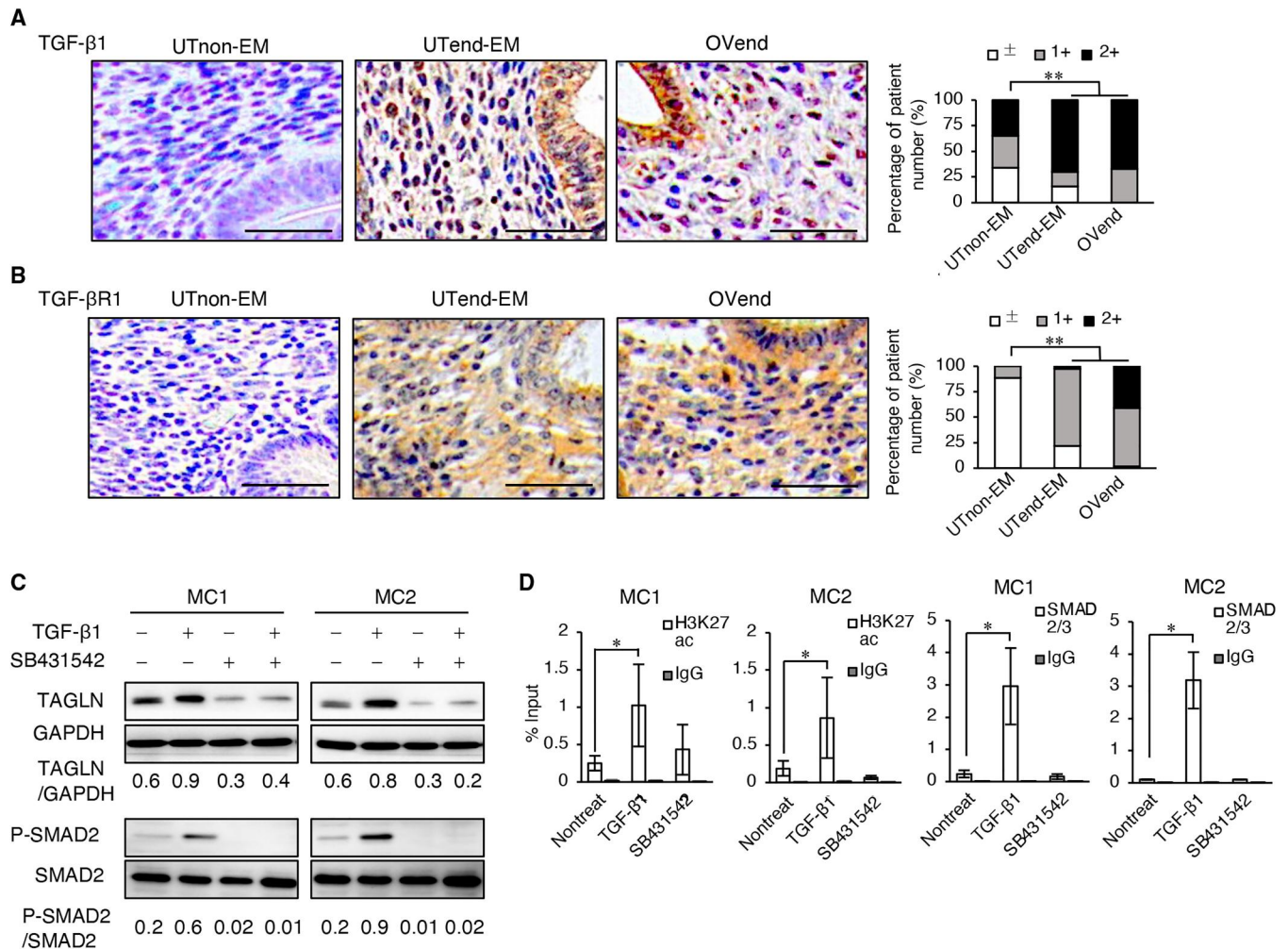


Fig. 3. TGF-β1 induces expression of TAGLN in vitro. (A and B) Representative images of immunohistochemical analysis of TGF-β1 (A) and TGF-βR1 (B) in UTnon-EM ($n = 44$), UTend-EM ($n = 37$), and OVend ($n = 49$). Scale bars, 100 μm (left). Tissues were classified by the IHC score of TGF-β1 (A) and TGF-βR1 (B) in stromal lesions of each sample (\pm , 0 to 100; 1+, 101 to 200; 2+, 201 to 300; right). (C) Abundance of TAGLN, phospho-SMAD2 (P-SMAD2), and total SMAD2 (SMAD2) in MC1 and MC2 cells after treatment with TGF-β1 (10 ng/ml) and SMAD2 inhibitor (SB431542, 1 μM). Ratios of TAGLN to GAPDH and P-SMAD2 to SMAD2 are shown below each gel image. (D) ChIP-qPCR analyses of H3K27ac and SMAD2/3 enrichment in the TAGLN enhancer and promoter regions, respectively. MC1 and MC2 cells were treated with either TGF-β1 or SB431542 (SMAD2-specific inhibitor). Error bars indicate SEM. * $P < 0.05$ and ** $P < 0.01$. Data were analyzed by Fisher's exact test (A and B) or two-tailed Student's t test (D), respectively.

To ensure that the endometriotic lesions were stably established in all recipient mice regardless of *F. nucleatum* infection, 8 mg of endometrial tissues were used for this transfer model. In the recipient endometriotic lesions, *F. nucleatum* was also observed, as was seen in the donor uterus (Fig. 5C). More abundant M2 macrophage infiltration, expression of TGF-β1, and TAGLN-positive myofibroblasts were observed in both the endometrial stromata of *F. nucleatum*-infected donor uteri and the endometriotic lesions established from *F. nucleatum*-infected uteri relative to the controls ($P < 0.01$; Fig. 5, D to G, and fig. S10B). Immunofluorescence analysis revealed infiltration of *F. nucleatum* organisms colocalized with TAGLN-positive cells in the *F. nucleatum*-infected endometrial stroma (Fig. 5H). High TAGLN protein expression was observed only in stromal cells but not in the epithelial cells in both the donor uterus and endometriotic lesions after infection with *F. nucleatum* (Fig. 5H). *F. nucleatum*-infected endometrium showed

high TGF-β1 abundance in the stroma with TAGLN expression (fig. S10C). In comparison with *F. nucleatum*, *L. iners* did not lead to M2 macrophage infiltration, induction of TGF-β1, or increased numbers of TAGLN-positive myofibroblasts after bacterial injection (Fig. 6, A to D, and fig. S10B). Consequently, *L. iners* injection did not facilitate development of endometriotic lesions relative to controls (Fig. 6E). We also tested the ability of a different Gram-negative bacterium, *Escherichia coli*, to form endometriotic lesions using the mouse model. However, this organism had no effect on numbers and weights of endometriotic lesions, similar to *L. iners* (Gram-positive bacteria) (fig. S10D). These data support *F. nucleatum* as a candidate bacterium associated with establishment of endometriosis.

In the clinical setting, the presence of *Fusobacterium* in the vaginal swab samples from patients with endometriosis was significantly greater than from patients without endometriosis ($P = 0.023$;

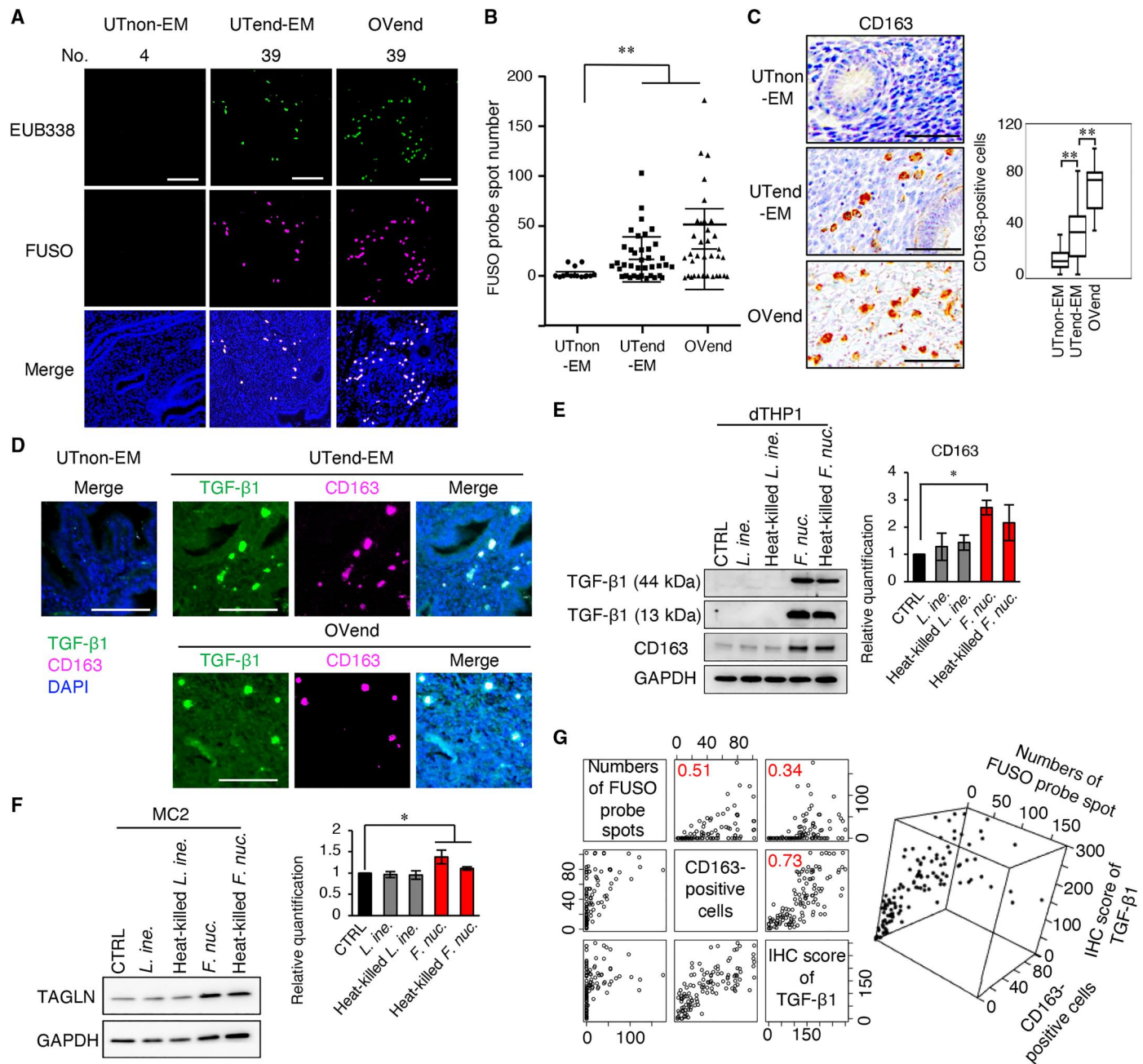


Fig. 4. *Fusobacterium* infection influences the microenvironment of the endometrium. (A) FISH analysis using the EUB338 probe for whole bacteria (green) and FUSO for *Fusobacterium* species (magenta) in UTnon-EM, UTend-EM, and OVend. Nuclei were stained with DAPI (blue). Patient numbers (No.) correspond to table S1. (B) Quantification of the numbers of FUSO probe spots in (A) ($n = 42$ in each group). (C) Abundance of CD163 in each tissue ($n = 42$, left). Middle horizontal line inside the box indicates the median value. Bottom and top of the box indicate the 25th and 75th percentiles, respectively. Ends of the whiskers indicate the minimum and maximum of all data, respectively (right). (D) Immunofluorescence staining of TGF-β1 (green) and CD163 (magenta) in UTnon-EM, UTend-EM, and OVend. Nuclei were stained with DAPI (blue). (E) Abundance of TGF-β1 (44-kDa precursor and 13-kDa cleaved mature proteins) and CD163 in dTHP1 cells cocultured with *F. nucleatum* (*F. nuc.*), *L. iners* (*L. ine.*), or heat-killed *F. nuc.* or *L. ine.*, as analyzed by Western blotting (left). The relative protein expression of CD163 to GAPDH was quantified (right). (F) Abundance of TAGLN in MC2 cells treated with the indicated conditioned medium (left). The relative protein expression of TAGLN to GAPDH was quantified (right). (G) Dot plot analysis between amounts of *Fusobacterium*, CD163-positive cells, and TGF-β1 in UTnon-EM ($n = 42$), UTend-EM ($n = 37$), and OVend ($n = 42$). The x, y, and z axes indicate the numbers of FUSO probe spots, numbers of CD163-positive cells, and IHC scores of TGF-β1. Pearson's correlation coefficients are shown in the upper left of each square. Error bars indicate 95% confidence interval (B) and SD (E and F). * $P < 0.05$, ** $P < 0.01$. Data were analyzed by Wilcoxon rank-sum test (B) and two-tailed Student's t test (C and E) and one-way ANOVA (F), respectively. Scale bars, 100 μm.

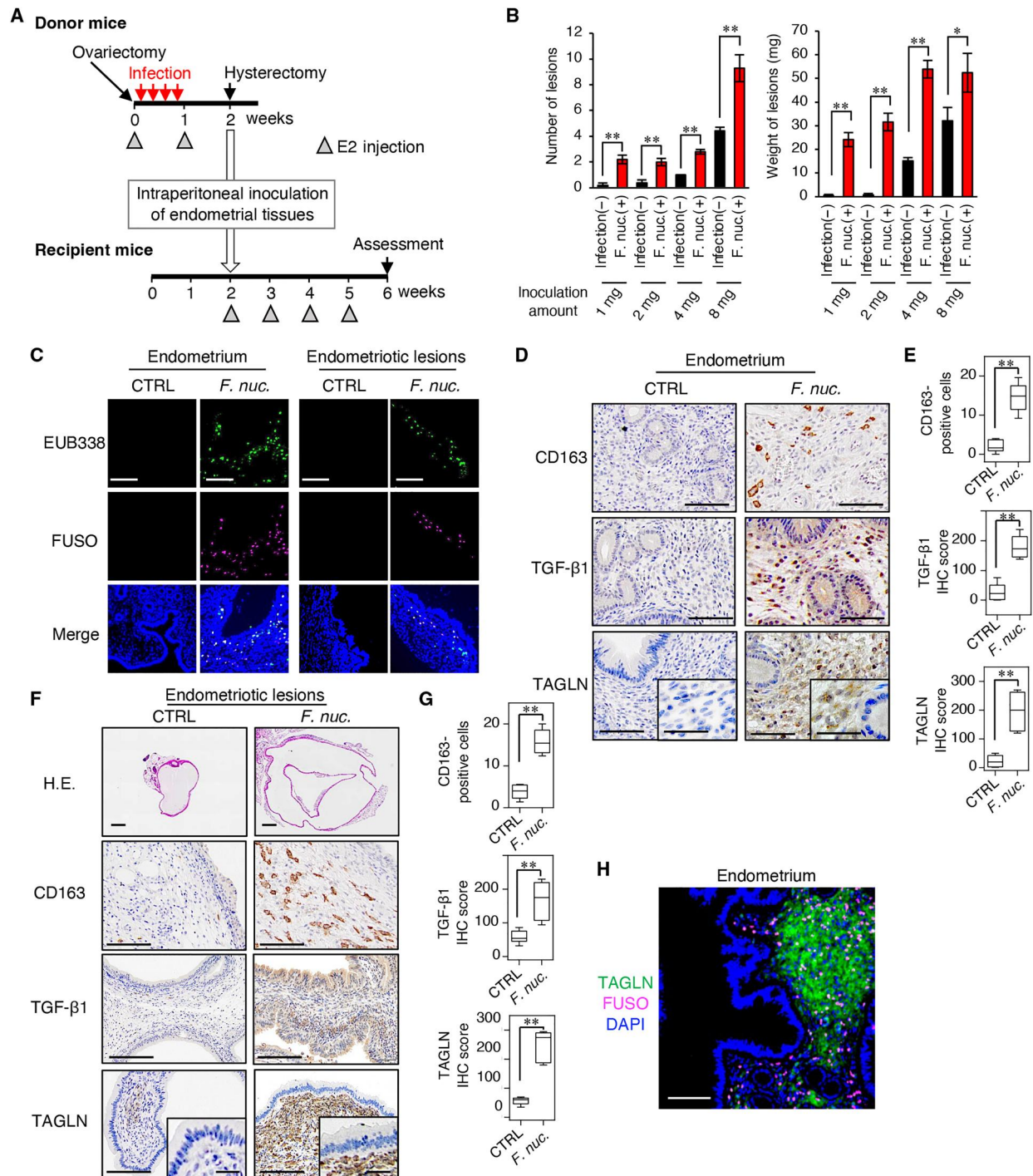


Fig. 5. *F. nucleatum* infection promotes endometriosis in mice. (A) Donor mice were transvaginally infected with *F. nucleatum* (*F. nuc.*) or *L.iners* (*L. ine.*) (red arrow). Endometrial tissues were intraperitoneally injected into recipient mice (white arrow). Gray triangles indicate 17β-estradiol treatments. To ensure the endometriotic lesions established in all the recipient mice, 8 mg of endometrial tissue were inoculated (C to H). (B) Number and weights of lesions from recipient mice processed in (A) ($n = 5$ in each group). (C) Detection of *Fusobacterium* with EUB338 (green) and FUSO (magenta) probes in endometria of donor mice infected without and with *F. nuc.* (left: CTRL and *F. nuc.*, respectively) and endometriotic lesions (right: CTRL and *F. nuc.*, respectively). DAPI (blue). Scale bars, 100 μm. (D and E) Presence of CD163, TGF-β1, and TAGLN in endometria from the infected donor mice. Scale bars, 50 μm. Numbers of infiltrated macrophages and IHC scores of TGF-β1 and TAGLN are shown in the boxplot ($n = 6$ in each group). Middle horizontal line inside the box indicates the median value. Bottom and top of the box indicate the 25th and 75th percentiles, respectively. Ends of the whiskers indicate the minimum and maximum of all data, respectively. (F and G) Presence of CD163, TGF-β1, and TAGLN in endometriotic lesions. Scale bars, 500 μm (H.E., hematoxylin and eosin) and 50 μm (CD163, TGF-β1, and TAGLN). Numbers of infiltrating macrophages and IHC scores of TGF-β1 and TAGLN are shown in the boxplot ($n = 6$ in each group). (H) Immunofluorescence of TAGLN (green) and *Fusobacterium* (magenta) in the endometria from infected mice. Nuclei were stained with DAPI (blue). Scale bars, 100 μm. $**P < 0.01$. Data were analyzed by two-tailed Student's *t* test. $*P < 0.05$.

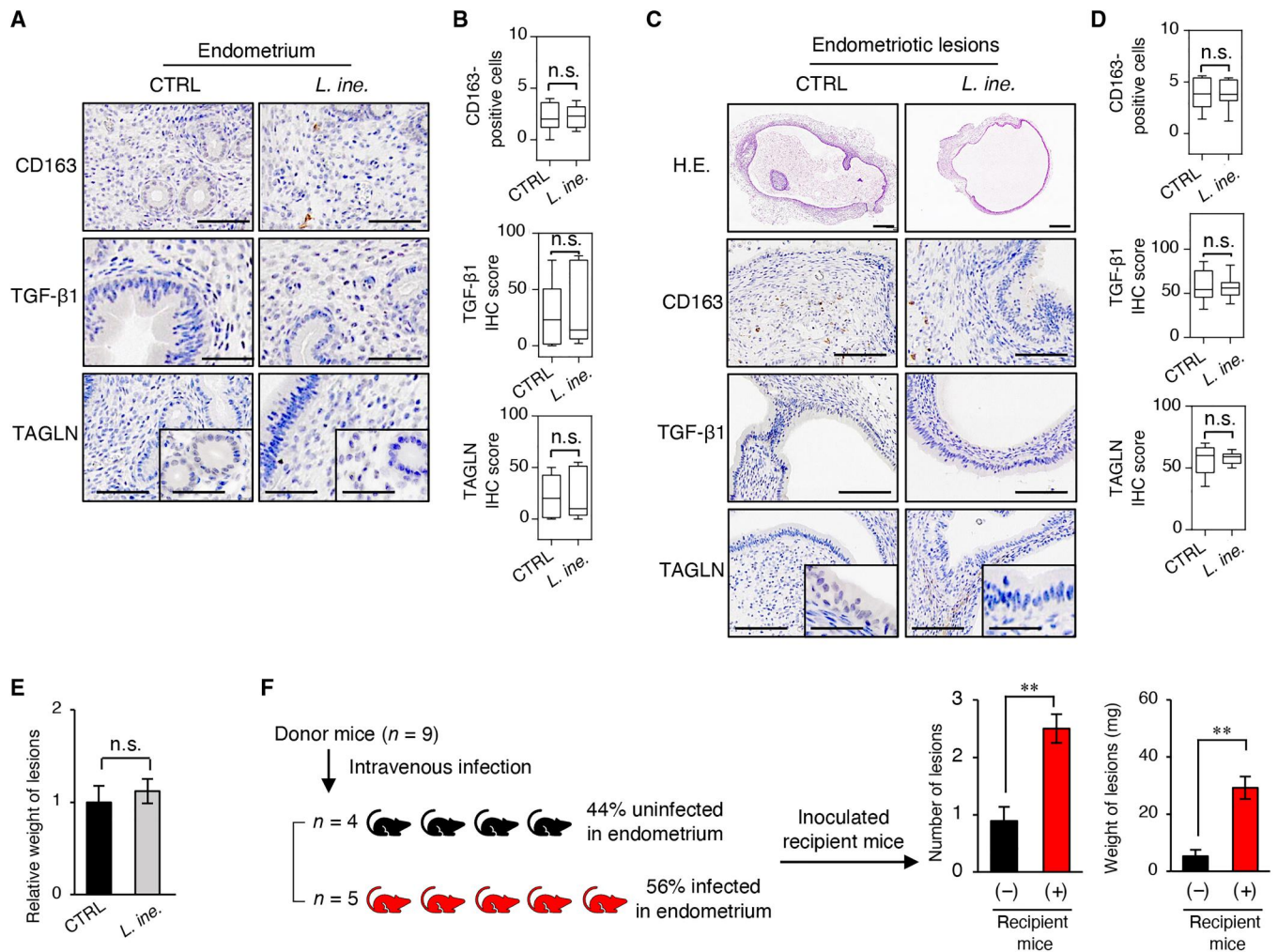


Fig. 6. Effects of bacterial infection in a syngeneic mouse model of endometriosis. To ensure that the endometriotic lesions were established in all the recipient mice, 8 mg of endometrial tissue were inoculated (A to D). Donor mice were transvaginally infected with *L. iners* (*L. ine.*) as is illustrated in Fig. 5A (A to D). (A) Presence of CD163, TGF-β1, and TAGLN in endometria from the infected mice. Scale bars, 50 μm. (B) Numbers of infiltrated macrophages and IHC scores of TGF-β1 and TAGLN are shown in the boxplot ($n = 6$ in each group). (C) Presence of CD163, TGF-β1, and TAGLN in endometriotic lesions of recipient mice. Scale bars, 500 μm (H.E.) and 50 μm (CD163, TGF-β1, and TAGLN). (D) Numbers of infiltrating macrophages and IHC scores of TGF-β1 and TAGLN are shown in the boxplot ($n = 6$ in each group). (E) Relative weight of endometriotic lesions from recipient mice processed in Fig. 5A ($n = 6$ in each group). (F) Infection rate of *F. nucleatum* (*F. nuc.*) in the endometria of donor mice after intravenous injection. The numbers (left graph) and weights (right graph) of each endometriotic lesion from recipient mice. (-), $n = 9$ in the uninfected group and (+), $n = 12$ in the infected group. Uninfected group indicates donors without presence of *F. nuc.* in their endometrial tissues even after intravenous injection of *F. nuc.* The amount of inoculation in Fig. 6F was 2 mg. Error bars indicate SEM (E and F). $**P < 0.01$; n.s., not significant. Middle horizontal line inside the box indicates the median value. Bottom and top of the box indicate the 25th and 75th percentiles, respectively. Ends of the whiskers indicate the minimum and maximum of all data, respectively. Data were analyzed by two-tailed Student's *t* test.

table S8). However, hematogenous transmission of *Fusobacterium* from the oral cavity to the uterus is also a possible route (41). Inoculation of donor BALB/c female mice with *F. nucleatum* via the jugular vein showed that 56% exhibited *F. nucleatum* colonization of the endometrium after 2 weeks (Fig. 6F). Endometriotic lesions established from the *F. nucleatum*-positive endometrial tissues were significantly larger than those from the *F. nucleatum*-negative tissues in this hematogenous transmission model ($P < 0.01$; Fig. 6F).

To examine the requirement for TAGLN-expressing fibroblasts in endometriosis formation after *F. nucleatum* infection in vivo, TAGLN was depleted by siRNA in the tissues from *F. nucleatum*-infected uteri of donor mice. Depletion of TAGLN significantly

reduced the numbers and weights of endometriotic lesions in comparison with the tissues treated with control siRNA ($P < 0.01$; fig. S11, A to D). Reciprocally, forced expression of TAGLN in tissues from donor uteri without *F. nucleatum* infection facilitated the increased numbers and weights of endometriotic lesions in vivo (fig. S11, E to H). These data implicated TAGLN protein expression in endometriosis after *F. nucleatum* infection.

Antibiotic treatment that eradicates *F. nucleatum* results in reduced endometriosis in a mouse model

Last, we explored the effects of antibiotic treatment to eradicate *F. nucleatum* in the syngeneic mouse model. Two different types of

antibiotics, metronidazole (MZ) and chloramphenicol (CP), to which *F. nucleatum* is sensitive, were administered transvaginally every day for 5 days after infection was established in donor mice (fig. S12A). After a week of antibiotic treatment, *F. nucleatum* infiltration was no longer present, and M2 macrophage infiltration, TGF- β 1 expression, and TAGLN expression were all decreased in both the endometria of donor mice and endometriotic lesions in recipient mice (fig. S12, B to D). Consistently, recipient mice, which received endometrium from *F. nucleatum*-infected donor mice treated with either MZ or CP antibiotics, developed significantly fewer endometriotic lesions weighing less than in the control group without antibiotics ($P < 0.01$; fig. S12E).

We further explored the effects of antibiotic treatments 3 weeks after the inoculation of endometrium, when the endometriotic lesions had already developed (Fig. 7, A and B). MZ or CP was administered orally for 5 days to mice with endometriotic lesions established from *F. nucleatum*-infected uteri. Antibiotic treatment decreased the amount of *F. nucleatum*, M2 macrophage infiltration, TGF- β 1 abundance, and TAGLN protein expression in the endometriotic lesions 21 days after initiation of treatment, but not after only 1 day (Fig. 7, B and C, and fig. S13, A and B). Antibiotic treatment resulted in a significant reduction in the weights of endometriotic lesions after 21 days of treatment ($P > 0.05$ and $P < 0.01$, respectively; Fig. 7, D and E). Together, these data suggest that MZ or CP antibiotic treatment may facilitate treatment of endometriosis.

DISCUSSION

In this study, we further the understanding of the pathogenesis of endometriosis by showing that *Fusobacterium* infection of the endometrium may contribute to disease. Increased numbers of myofibroblasts with high TAGLN expression were found in the endometrial microenvironment where *Fusobacterium* was present. The reason why *Fusobacterium* preferentially infects the endometria of some patients is uncertain. Some work has shown intrauterine infection of *F. nucleatum* due to hematogenous transmission of the bacteria from the oral cavity. Such transmission mostly occurs during pregnancy, when blood flow to the placenta is generally increased (42). Because patients with endometriosis are often nonparous, transmission through the vagina may also be considered. The presence of *Fusobacterium* in the vaginal swab samples from patients with endometriosis was significantly greater than from patients without endometriosis ($P = 0.023$; table S8), supporting the possibility of a vaginal transmission route. Menstrual cycle-associated changes in mucin conformation and immune cell function, both barriers against bacterial infection, have been demonstrated in the female reproductive tract, which is associated with the individual's susceptibility to infections (43, 44). *F. nucleatum* appears to damage the intestinal barrier of tumors and induce aberrant inflammation (45–47). These pathogenic roles of *Fusobacterium* may be due to its strong adhesion to epithelial tissues and its invasive abilities (48, 49).

We found that *F. nucleatum*, even when heat-killed, effectively stimulated the production of TGF- β 1 from M2 macrophages and activated TGF- β signaling in vitro. A recent study showed that Gram-negative bacteria, including *F. nucleatum*, induce innate immune responses via recognition by Toll-like receptor 4 (TLR4) of their cell walls, which are composed of lipopolysaccharide (41).

This enhances M2 macrophage polarization within the tumor immune microenvironment (50). Thus, *Fusobacterium* infection appears to create a TGF- β 1 signaling-enriched environment in the endometrium.

TAGLN is also expressed in certain other fibroblasts, such as cancer-associated fibroblasts (CAFs), which have a role in creating extracellular matrix structures and in metabolic and immune reprogramming of the tumor microenvironment (6). Comprehensive scRNA-seq analysis revealed that one subtype of CAF in the microenvironment of colorectal cancer expressed cytoskeletal genes and markers of activated myofibroblasts, such as *ACTA2*, *TAGLN*, and *PDGFA*, whereas another subtype expressed genes related to extracellular matrix remodeling (51). Fibrosis of the surrounding tissue is a hallmark of peritoneal or ovarian endometriosis. Despite some similarities between fibrosis-associated myofibroblasts and CAFs, invasive and proliferative abilities appear to be less potent in endometriosis than malignancy (6, 52). Although functional differences between these two types of fibroblasts are yet to be clearly defined at the molecular basis (6), both fibrosis-associated myofibroblasts and CAFs nevertheless gain enhanced proliferative properties and are functionally diverse populations different from other subtypes of fibroblasts (6).

Two theories of the pathogenesis of ovarian endometriomas have been considered: invagination of shed endometrial cells derived from retrograde menstruation into the ovarian cortex and surface epithelial transdifferentiation to endometrial-lined ovarian cysts (coelomic metaplasia) (3). Our data are consistent with the former. However, it is also plausible that coelomic metaplasia may be caused by *Fusobacterium* infection. To date, the stimuli causing transformation of coelomic epithelium into endometrial-type glands remain unidentified (53). *Fusobacterium* may trigger the transdifferentiation of ovarian surface epithelial cells. A recent study showed that bacterial infection induced transdifferentiation of epithelial cells during colon tumorigenesis (54). The possibility that *Fusobacterium* is a trigger of metaplasia needs to be explored in the future.

We investigated the roles of *F. nucleatum* and TAGLN in the initiation and development of endometriosis using a mouse model, because *F. nucleatum* is not present in laboratory mice, and TAGLN is well conserved between humans and mice (55). Despite being the most frequently applied animal model valuable for the study of endometriosis, mice do also have some limitations. Endometriosis is a condition in which endometrial tissue aberrantly grows ectopically. However, mice lack a menstrual cycle and do not develop spontaneous endometriosis (56). Therefore, endometriotic lesions in our mouse models have to be induced by peritoneal injection of minced endometrial tissue, a limitation of which is that this contains myometrial cells that are not present in refluxed menstrual tissue. Using the mouse model that we used in the current study, earlier work has revealed several important features of the human disease, including the hormonal resistance of endometriosis (57–59). Recently, Greaves *et al.* (60) developed a mouse model of endometriosis that closely reflects the human condition and has revealed that immune complement in the menstrual endometrium contributes to the appearance of pathology. In this model, inoculated endometrium is removed from the myometrial layer. Further validation of these findings using this model will need to be conducted in the future.

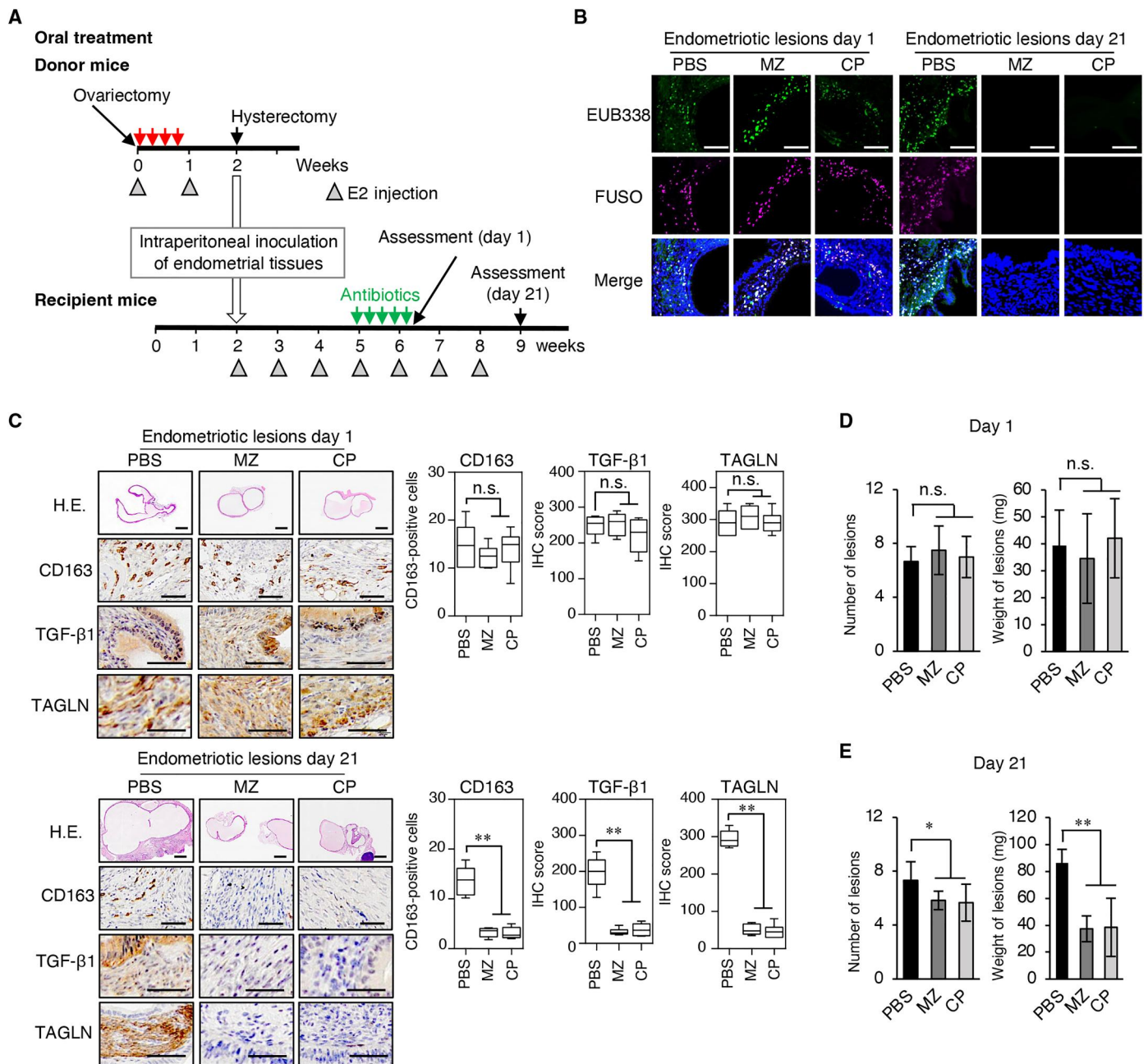


Fig. 7. Antibiotic treatment that eradicates *F. nucleatum* reduces endometriotic lesion weight in mice. (A) Donor mice were infected with *F. nucleatum* (red arrow). Endometrial tissues were injected into the recipients 1 week after infection (white arrow). To ensure that the endometriotic lesions established in all the recipient mice, 8 mg of endometrial tissue were inoculated (A to E). Three weeks after inoculation, recipient mice were treated with oral antibiotics for 5 days (green arrow). Gray triangles indicate 17 β -estradiol treatments. (B) Detection of *Fusobacterium* with EUB338 (green) and FUSO (magenta) probes in endometriotic lesions of recipient mice at day 1 (left) and day 21 (right) after treatment with either MZ or CP. Nuclei are stained with DAPI (blue). Scale bars, 100 μ m. (C) Presence of CD163, TGF- β 1, and TAGLN in endometriotic lesions of recipients at day 1 (top left) and day 21 (bottom left) after treatment. Scale bars, 1 mm (H.E.) and 50 μ m (CD163, TGF- β 1, and TAGLN). Numbers of infiltrated macrophages and IHC scores of TGF- β 1 and TAGLN are shown in boxplots (right, $n = 6$ in each group). Middle horizontal line inside the box indicates the median value. Bottom and top of the box indicate the 25th and 75th percentiles, respectively. Ends of the whiskers indicate the minimum and maximum of all data, respectively. (D and E) Numbers (left) and weights (right) of endometriotic lesions in recipients treated with each antibiotic ($n = 6$ in each group) at day 1 (D) and day 21 (E). Error bars indicate SD (D and E). * $P < 0.05$ and ** $P < 0.01$. Data were analyzed by one-way ANOVA.

Treatment options for endometriosis are currently based on hormonal therapy, such as long-term ovulation suppression (52). However, creating a relatively hypoestrogenic environment can lead to adverse effects, and women cannot become pregnant during treatment (5). Surgical treatment is generally necessary for intractable pelvic pain. However, a high recurrence rate is a major concern after surgical removal of endometriotic lesions (52). Our data reveal a potential pathogenic mechanism of endometriosis involving *Fusobacterium* infection, and eradication with MZ or CP could represent an option to improve treatment of this disease. Consistent with our findings, a recent empirical study showed that MZ treatment reduced the growth of endometriotic lesions in a mouse model, although the potential involvement of pathogenic bacteria and the underlying mechanisms were not elucidated (61). Thus, combining antibiotics with other therapeutics, such as hormone treatments, might be another approach and will hopefully be examined in future clinical trials.

We found that 64% of patients with endometriosis had *Fusobacterium* in their endometria, supporting the idea that endometriosis is a multifactorial disease and that its pathogenesis is difficult to ascribe to a single factor. In addition, bacterial infections other than *Fusobacterium* might also be involved in causing endometriosis. Recent studies have shown that various different bacteria may be present in the urine, vagina, or uterus from patients with endometriosis, although *F. nucleatum* has not been identified as a causal bacterium for the disease (62–65). Because the amount of bacteria in the uterus is quite low (17), differences in the methodology used in these studies may explain the divergent results regarding the microbiota repertoire. Nevertheless, we documented higher frequency of *Fusobacterium* in both the endometrium and ovarian endometriotic tissues and documented pathogenic effects in endometriosis infected with pure cultured *F. nucleatum* in an in vivo mouse model. Furthermore, antibiotic treatment effective against *F. nucleatum* reduced lesion weight. Therefore, *Fusobacterium* may have a pathogenic role in endometriosis rather than simply flourishing in the environment of the endometrium in reproductive-age women with endometriosis.

This study has some limitations that need to be considered when interpreting the results. First, as already mentioned, the study lacks direct evidence supporting the hypothesis that the presence of *Fusobacterium* in the endometrium promotes endometriosis after retrograde menstruation. Considering the many studies documenting mechanisms responsible for endometriosis (1–5), further precise studies are needed. Second, clinical studies are required to ascertain whether treatment with antibiotics against *Fusobacterium* represents a bona fide effective treatment for patients with endometriosis.

In conclusion, we presented evidence that myofibroblasts expressing TAGLN promote endometrial cell survival at ectopic sites. These cells are induced by TGF- β signaling, which can be activated by *Fusobacterium* infection. Although further studies are needed, our data suggest that targeting *Fusobacterium* in the endometrium by antibiotic treatment may be a therapeutic option for patients with endometriosis.

MATERIALS AND METHODS

Study design

We designed a series of studies to identify mechanisms involved in the development of endometriosis caused by the phenotypic

transition of endometrial fibroblasts induced by TGF- β and to test the hypothesis that endometrial *Fusobacterium* infection promotes these phenotypic transitions. We first designed an observational study in humans to identify genes specifically expressed by endometrial fibroblasts in patients with endometriosis. We next designed a functional study of human endometrial fibroblasts strongly expressing TAGLN. We then proceeded to investigate upstream targets to determine whether the phenotypic transition was caused by TGF- β and systemic and local inflammatory responses after *Fusobacterium* infection. We finally designed in vivo analyses to determine whether *Fusobacterium* infection promotes endometriosis development in mice and to explore the effectiveness of antibiotics as a nonhormonal treatment for endometriosis. Mice were randomized to their respective treatment groups. Pathological quantification, microarray, and scRNA-seq analyses were performed by blinded investigators. Analysis of experimental data from the mice was not blinded. All experiments were performed in triplicate. Although formal statistical methods were not used to predetermine sample size, sample sizes were chosen on the basis of estimates from pilot experiments and previously published results.

Animal experiments were performed using protocols approved by the Institutional Animal Care and Use Committee of Nagoya University Graduate School of Medicine (no. 20165). All samples were collected with written informed consent after approval by the Institutional Review Board of the Nagoya University Graduate School of Medicine (nos. 2014-0134, 2017-0497, 2017-0503, and 2021-0178).

Human tissue samples

Samples from all patients were obtained from Nagoya University Hospital and Toyota Kosei Hospital in Japan. Seventy-six patients without endometriosis and 79 patients diagnosed with endometriosis were enrolled in this study. Paired primary endometrial and endometriosis samples were taken from the 79 patients who underwent surgical removal of the uterus together with the endometriotic lesions. Because the uterus is retained during the surgical treatment in younger women for possible future pregnancies, the median age of the patients studied here was >40 years. In the control group without endometriosis, patients had undergone surgery for leiomyoma, adenomyosis, cervical dysplasia, or cervical cancer and had no history of endometriosis. Detailed patients' information is provided in table S1. The vaginal samples were collected using cotton swab (DNA/RNA Shield Collection Tube With Swab, ZYMO RESEARCH) to absorb vaginal secretions. All patients had regular menstrual periods and had not received any hormonal treatment for at least 3 months before surgery or at the time of collecting the samples. No patients had received treatment with antibiotics or anti-inflammatory drugs for 1 month before surgery or at the time of collecting the samples. Primary fibroblasts were collected from each sample after shaking the sample for 1 hour at 37°C in Dulbecco's modified Eagle's medium (DMEM)/F12-containing collagenase (200 U/ml; Thermo Fisher Scientific) and straining through a 40- μ m nylon mesh as was reported previously (21). Primary human mesothelial cells were obtained from the tumor-free omenta of female patients with serous adenocarcinoma without genetic modification (66).

Cell lines

The UTnon-FB lines (MC1 and MC2) have been established previously (67). The OVend-FB lines (SC8 and SC10) were established in the current study using the same method as used for MC1 and MC2 (67). Briefly, all four cell lines were immortalized by transfection with telomerase reverse transcriptase (TERT), cyclin D1, and mutant CDK4 genes. Clinical data of the patients from which the four cell lines were derived are shown in table S9. Immortalized fibroblasts were maintained in DMEM/F12 supplemented with 10% fetal bovine serum (FBS; Thermo Fisher Scientific) and 1% antibiotic-antimycotic solution that includes penicillin, streptomycin, and amphotericin (Anti-anti, Thermo Fisher Scientific). The human monocyte cell line THP-1 was purchased from the JCRB Cell Bank (JCRB0112.1, human acute monocytic leukemia cell line, Osaka, Japan) and maintained in RPMI 1640 medium supplemented with 10% FBS and 1% Anti-anti. The cell line was authenticated through short tandem repeat profiling by the JCRB Cell Bank and was mycoplasma-free. All cells were cultured at 37°C in a humidified incubator with 5% CO₂.

Plasmid construction

A human TAGLN vector, pcDNA3.4-TAGLN, and an N-terminal Flag-tagged human TAGLN vector, pcDNA3.4-Flag-TAGLN-FL, were constructed by inserting a full-length human TAGLN cDNA fragment from pCMV-SPORT6.1-hTAGLN (IRAK141P09, RIKEN, Japan) into pcDNA3.4. A partial deletion construct of TAGLN, pcDNA3.4-Flag-TAGLN-ΔCLI, was created by inverted PCR using PrimeSTAR Max DNA Polymerase (TAKARA) and ligation of the PCR products. pCAG-mTAGLN was constructed by inserting a full-length mouse *Tagln* cDNA into a pCAG-HIVgp vector using In-Fusion HD Cloning Kits (TAKARA). The pCAG-green fluorescent protein (GFP) vector was used as a control. The primer sequences for the inverted PCR and mouse TAGLN are shown in table S10. All constructs were verified by Sanger sequencing.

Cell manipulation

Transfections with the plasmids and siRNAs were carried out using Lipofectamine 3000 (Thermo Fisher Scientific) or ScreenFect A Plus (FUJIFILM Wako Pure Chemical) according to the manufacturer's protocol. We used 50 nM siRNA targeting TAGLN (#1, si14039 and #2, si14040; Thermo Fisher Scientific) or negative control siRNA (Silencer Select Negative Control siRNA, 4390844, Thermo Fisher Scientific). Cells stably overexpressing TAGLN were generated by transfecting MC1 and MC2 with pcDNA3.4-TAGLN, followed by geneticin selection (100 µg/ml; Thermo Fisher Scientific).

Bacterial strains and culture

F. nucleatum (JNBP_02614), *L. iners* (GAI_11032), and *E. coli* K-12 (GTC_2003) were obtained from Gifu University Center for Conservation of Microbial Genetic Resource, Organization for Research and Community Development, Japan (<https://pathogenic-bacteria.nbrp.jp/bacteria/bacteriaAllItemsList.jsp>). *F. nucleatum* and *L. iners* were first cultured under anaerobic conditions at 37°C in Brucella agar (Kyokutoseiyaku). We then used liquid cultures based on brain heart infusion (Nissui Pharmaceutical Co) broth medium, supplemented with hemin (10 µg/ml, Thermo Fisher Scientific), menadione (5 µg/ml, Nacalai Tesque), L-cysteine (1 µg/ml, Sigma-Aldrich),

and resazurin (2 µg/ml, FUJIFILM Wako Pure Chemical) as an anaerobic indicator. *F. nucleatum* colonies were transferred to the liquid culture medium and maintained at 37°C under anaerobic conditions with constant stirring on a magnetic stirrer. The bacterial cell concentrations were measured by assessing optical density at 660 nm (Miniphotofluorimeter, TAITEC) or McFarland standard 0.5 (BioMérieux). *E. coli* K-12 was cultured under aerobic conditions at 37°C in L-Broth agar (MP Biomedicals).

Animal experiments

We used an endometriosis model in which endometrial tissues from estrus-stage donor mice are intraperitoneally inoculated into the recipient mice (40). Endometriosis induction surgery was performed using 6-week-old BALB/c female mice (Japan SLC, Shizuoka) given 17β-estradiol (100 µg/kg per mouse per week; Fuji Pharma) subcutaneously after ovariectomy of donor mice. Endometrial tissues were collected from one donor, minced using fine scissors, and injected intraperitoneally by syringe into two recipients, followed by ovariectomy of recipient mice under anesthesia and pain control and subcutaneous injection with 17β-estradiol (100 µg/kg) once a week. Four weeks after the intraperitoneal inoculation, endometriotic lesions of the recipient mouse were detected as a cyst composed of ERα- and ERβ-positive stromal cells (fig. S10A) (57). Endometriotic lesions, which were located on the superficial layers of the peritoneum, mesentery, and near the ovaries, were counted and measured by a micro-weighing instrument (ENTRIS64-1S, Sartorius) after removal from the abdominal cavity. All mice were maintained in a specific pathogen-free biosafety level 2 biohazard facility. Experimental mice were cohoused and exposed to a 12-hour light/12-hour dark cycle with unrestricted access to water and food. The ambient temperature was restricted around 25°C, and the room humidity ranged from 40 to 70%.

Animal experiment 1

Four different amounts of endometrial tissues— $1/16$ (1 mg), $1/8$ (2 mg), $1/4$ (4 mg), and $1/2$ uterus (8 mg)—were titrated to determine the appropriate amount to use for the endometriosis formation model. For each amount, five mice were included in both the *F. nucleatum*-uninfected and *F. nucleatum*-infected groups. Because we intended to examine and compare differences in the established endometriotic lesions inoculated from the donor mice with and without *Fusobacterium* infection, a minimally sufficient amount of endometrial tissues was used in most of our experimental condition (almost 8 mg).

Animal experiment 2

Transvaginal bacterial infections of donor mouse endometrium were performed four times over 1 week beginning at 6 weeks of age. A sham group was treated with phosphate-buffered saline (PBS), and for infection, *F. nucleatum*, *L. iners*, or *E. coli* K-12 at 10^7 colony-forming units (CFUs)/10 µl of PBS per day were applied intravaginally. A schema of the mouse endometriosis model with transvaginal infection is shown in Fig. 5A ($n = 6$ each for four experimental groups: CTRL, *L. iners*, *E. coli* K-12, and *F. nuc.*). We administered a 2- or 8-mg amount of endometrial tissues for each experiment.

Animal experiment 3

For hematogenous administration, 10^7 CFUs of *F. nucleatum* in 10 µl of PBS were injected into the jugular veins of mice using a 34-gauge microneedle. Bacterial injections into donor mice were performed four times over 1 week. One week after infection, 2 mg of the

donor mouse endometrial tissue were inoculated into the recipient mice. Before inoculation, a part of the donor tissue was examined for the presence of *F. nucleatum* by FISH analysis. No mouse experienced a deterioration in health after the hematogenous administration of *F. nucleatum*.

Animal experiment 4

Antibiotics for treating the endometria of donor mice, containing MZ (17 µg per mouse per day; FUJIFILM Wako Pure Chemical) or CP (7 µg per mouse per day; Sigma-Aldrich), were introduced transvaginally every day for 5 days after infection with *F. nucleatum*. Endometrial tissues were intraperitoneally injected into the recipient mouse 1 week after antibiotic treatments. A schema for the mouse transvaginal antibiotic treatment model is shown in fig. S12A ($n = 6$ each for the three experimental groups: PBS, MZ, and CP). To treat endometriosis, 4 weeks after endometriosis induction surgery and *F. nucleatum* infection, mice were treated with antibiotics containing MZ (17 µg per mouse per day) or CP (7 µg per mouse per day) for 5 days by oral gavage. After antibiotic treatments, endometriotic lesions were harvested and evaluated for numbers and total weight. A schema for the mouse oral antibiotic treatment model is shown in Fig. 7A ($n = 6$ each for the three experimental groups: PBS, MZ, and CP).

Animal experiment 5

Electroporation was used to introduce pCAG-mTAGLN ($n = 4$ mice) or pCAG-GFP ($n = 4$ mice) control vectors and the overexpressed mouse-*Tagln* gene into the minced donor mouse uterus tissues without *Fusobacterium* infection. For electroporation, after five rectangular pulses (40 V, 5-ms duration with an interval of 50 ms) for 5 s, the direction of the electrical field was reversed, and three pulses were applied with identical settings (CUY700P2L and CUY701P5E, Nepa gene) (68). Electroporation was also used to perform *Tagln* knockdown experiments in the minced uteri from *Fusobacterium*-infected donor mice under the same conditions. siRNAs against mouse-*Tagln* (#1: SASI_Mm01_00135382, $n = 6$ mice and #2: SASI_Mm01_00135383, $n = 6$ mice; Sigma-Aldrich) or negative control siRNA (Silencer Select Negative Control siRNA, 4390844, Thermo Fisher Scientific; $n = 6$ mice) were used here. The efficiency of overexpression and depletion was validated after 24 hours by qPCR and Western blotting (fig. S11).

ChIP assay

Chromatin immunoprecipitation (ChIP) assays were performed according to previously published methods (69). UTnon-FB cell lines (MC1 and MC2) were treated with either TGF-β1 or SB431542 for 48 hours. Ten percent of each lysate was used as an input control. The putative enhancer and promoter regions were identified by the enrichment of H3K27ac and SMAD2/3 in fibroblasts by reference to a public database (SCREEN database, <https://screen.encodeproject.org/>; fig. S7B) (70). Primer sets for ChIP-qPCR are shown in table S10. We used anti-H3K27ac (39133, Active Motif) and anti-SMAD2/3 (#8685, Cell Signaling Technology) antibodies for target lesions and anti-IgG (immunoglobulin G) (PM035, MBL International) antibody as the negative control.

Immunofluorescence

Cell cultures were fixed with 2% paraformaldehyde for 10 min. After incubating with 0.1% Triton X-100 on ice for 2 min, the cells were blocked for 15 min using 2% gelatin. Samples were washed with PBS/glycine and incubated with primary antibody

against TAGLN (ab14106, 1:100, Abcam, Cambridge, UK), αSMA (M0851, 1:100, Agilent Technologies, Santa Clara, CA), IL-6 (MAB2062, 1:25, R&D Systems, Minneapolis, MN or ab214429, 1:500, Abcam), or FLAG (F1804, 1:100, Sigma-Aldrich) or with control serum for 1 hour at room temperature. Cells were then incubated with 4',6-diamidino-2-phenylindole (DAPI; #4083, 1:1000, Cell Signaling Technology, Danvers, MA) and the combination of Alexa Fluor 488-labeled anti-mouse secondary antibody (A-11029, 1:500, Thermo Fisher Scientific) and Alexa Fluor 546-labeled anti-rabbit secondary antibody (A-11010, 1:500, Thermo Fisher Scientific) or the combination of Alexa Fluor 488-labeled anti-rabbit secondary antibody (A-11070, 1:500, Thermo Fisher Scientific) and Alexa Fluor 546-labeled anti-mouse secondary antibody (A-11018, 1:500, Thermo Fisher Scientific) for 45 min at room temperature. Coimmunostaining of tissue samples with anti-TAGLN and anti-IL-6 antibody, with anti-CD163 (ab182422, 1:100, Abcam) and anti-TGF-β1 (ab92486, 1:100, Abcam), or with anti-TAGLN and anti-TGF-β1 was performed using the Opal Multi-plex IHC Detection Kit (PerkinElmer, Waltham, MS) following the manufacturer's protocol. For the immunofluorescence negative control, we stained without primary antibody as a negative control. Images were acquired using a Leica DMI6000B. The integrated density of the fluorescent signal of cells was measured using ImageJ software using region of interest polygon selection (71). The IL-6 and TAGLN fluorescence score was calculated using the following equation: score = $\sum P_i(i)$, where i = intensity of staining (1, 2, or 3 as weak, moderate, or strong, respectively), and P_i is the percentage of stained cells for each intensity. We calculated the average fluorescence scores of at least five different fields of one section.

Immunohistochemistry

Staining was performed on 5-µm sections of mouse and human tissues. After deparaffinization, antigen retrieval was performed in a microwave oven in 10 mM sodium citrate buffer (pH 6.0) or tris/EDTA buffer (pH 9.0). After blocking in 3% H₂O₂ for 20 min, specimens were incubated with the primary antibodies as follows: TAGLN (ab14106, 1:200, Abcam), CD68 (M0876, 1:100, Agilent Technologies), CD163 (ab182422, 1:100, Abcam), TGF-β1 (ab92486, 1:100, Abcam), TGF-βR1 (ab31013, 1:200, Abcam), ERα (ab32063, 1:200, Abcam), ERβ (#PA1-310B, 1:50, Thermo Fisher Scientific), and CD10 (sc9149, 1:100, Santa Cruz Biotechnology). After subsequent incubation with horseradish peroxidase-conjugated secondary antibody, specimens were subjected to diaminobenzene (DAB) (Agilent Technologies) and hematoxylin staining. The TAGLN IHC score was calculated using the following equation: IHC score = $\sum P_i(i)$, where i = intensity of staining (positive equal to muscle cells: 0 or 1) and P_i is the percentage of stained cells. The TGF-β1 and TGF-βR1 IHC score was calculated using the following equation: IHC score = $\sum P_i(i)$, where i = intensity of staining (1, 2, or 3 as weak, moderate, or strong, respectively) and P_i is the percentage of stained cells for each intensity. We calculated the total TAGLN IHC scores or average TGF-β1 or TGF-βR1 IHC scores of at least five different fields of one section using an Olympus VS120 microscope at ×200 magnification.

Cytokine analysis

UTnon-FB cell lines (MC1 and MC2) were transfected with pcDNA3.4-TAGLN to overexpress TAGLN for 2 days. OVend-FBs (SC8 and SC10) were treated for 2 days with 50 nM siRNA targeting

TAGLN (#2; si14040) or negative control siRNA to knock down *TAGLN*. Cytokines secreted by the cells were detected in conditioned medium using RayBiotech Human Neuro Discovery Array C2 according to the manufacturer's instructions (RayBiotech Inc.). The signal intensity of each spot, which represents the secreted cytokines, was evaluated by subtracting the background and normalized to positive controls using ImageJ software.

Fluorescence in situ hybridization

FISH was performed using formalin-fixed paraffin-embedded endometrial and endometriosis specimens. Sections were hybridized with the 5' FAM-labeled universal bacterial probe EUB338 (30), the 5' Cy3-labeled *Fusobacterium* genus-specific probe FUSO (31), and the 5' Cy5-labeled *F. nucleatum*-targeted probe FUSO664 (32–34). The sequences of the FISH probes were obtained from probeBase (<http://probebase.csb.univie.ac.at/>): pB-00159 for EUB338, pB-00782 for FUSO, and pB-1346 for FUS664. A scrambled probe(5'-CAATTGGGCCCGCTTTAACCCAATCTC-3') served as the non-specific negative control. Slides were deparaffinized and treated with 0.2 M HCl for 20 min and then hybridized overnight with the indicated FISH probes at a concentration of 10 ng/μl at 56°C in hybridization buffer [0.9 M NaCl, 20 mM tris-HCl (pH 7.2), and 0.1% SDS]. Slides were washed for 20 min at 58°C in wash buffer [0.9 M NaCl and 20 mM tris-HCl (pH 7.2)]. Tissue sections were counterstained with DAPI and mounted. Coimmunostaining with the anti-*TAGLN* antibody and FISH probe (FUSO probe) was performed without antigen retrieval using the Opal Multi-plex IHC Detection Kit (PerkinElmer) following the manufacturer's protocol. Images were acquired using a Leica DMI6000B. Bacterial spots were counted by ImageJ software using polygonal region of interest selection. We calculated the total bacterial spot numbers in at least five different fields of one section.

Microarray analysis

RNA microarray assays were performed as described previously (72). The RNA was amplified into complementary RNA and labeled according to the Agilent One-Color Microarray-Based Gene Expression Analysis protocol (Agilent Technologies). Labeled samples were purified using RNeasy Mini Kits (Qiagen) and hybridized to SurePrint G3 Human Gene Expression 8x60K v3 array slides (G4851C, Agilent Technologies) at 65°C with rotation at 10 rpm for 17 hours. The arrays were scanned using an Agilent Microarray Scanner (G2565BA, Agilent Technologies). The scanned images were analyzed using Feature Extraction software, version 12.0 (Agilent Technologies), with background correction. Data analysis was performed with GeneSpring GX, version 14.9 (Agilent Technologies).

Single-cell analysis

Samples for scRNA-seq were prepared using the same digestion method as for the RNA microarray assays in this study. After removing the red blood cells, cell viability was quantified using the trypan blue exclusion method. Cell concentration was adjusted for targeted sequencing of 10,000 cells per sample using Chromium Single Cell 3' Reagent Kits v3.1 (10x Genomics) to prepare libraries. The libraries were sequenced in the Center for Omics and Bioinformatics, Graduate School of Frontier Sciences, University of Tokyo using the Novaseq 6000 system (Illumina). The fastq files were mapped to the reference genome provided by 10x Genomics (GRCh38).

The read count was quantified using the Cell Ranger version 6.0.0 count pipeline (10x Genomics) with default parameters. The following data analysis was performed with Python version 3.9.7 and Scanpy version 1.8.2. For quality control, cells with greater than 9000 or fewer than 2000 detectable genes or whose mitochondrial contribution exceeded 10% of transcripts were removed. After integrating UTnon-EM and OVend data, the expression profile was normalized to counts per 10,000 and then log-transformed. The highly variable genes (HVGs) were calculated using in-built functions (scanpy.pp.highly_variable_genes) with default parameters. Principal components analysis (PCA) was performed on the expression profile of HVGs, and batch effects were corrected using Harmony version 1.0. Dimension reduction was conducted with Uniform Manifold Approximation and Projection (UMAP). We performed Leiden clustering and manually annotated these clusters on the basis of marker genes; for epithelial cells, *EPCAM* and *KRT18*; for macrophages/monocytes, *CD68* and *MS4A7*; for T cells/NK cells, *CD2*, *CD3D*, *CD3E*, *CD3G*, *TRDC*, *KLRC1*, *FCGR3A*, and *CEACAM1*; for MAST cells, *KIT* and *TSPB2*; for endothelial cells, *AQP1*, *MTCT1*, *CDH5*, and *PECAM1*; for fibroblasts, *COL1A1*, *COL3A1*, and *COL1A2*.

Bacterial selection methods

We downloaded the publicly available raw data of the endometrial bacterial analysis of the target patients from the database [European Nucleotide Archive under study numbers PRJEB16013 and PRJEB21098; dataset from a previous study (17)] and reanalyzed them ourselves. Each datum was referenced to VITCOMIC2 (<http://vitcomic.org/>) to identify the bacterial genera. The read count of each bacterium was divided by the total bacterial read count to calculate the percentage of each bacterium present. The top five bacterial genera significantly present in UTend-EM compared with those without endometriosis were selected ($P < 0.01$; table S6).

Bacterial infection experiments in vitro

THP-1 monocytes were differentiated into macrophages (dTHP1) by treatment with 10 nM phorbol 12-myristate 13-acetate (PMA) (Sigma-Aldrich) for 48 hours (73). For bacterial and dTHP1 coculture experiments, dTHP1 cells were mixed with live or heat-killed *F. nucleatum* or *L. iners* at a multiplicity of infection (MOI) of 10 bacteria:1 dTHP1 cell for 48 hours. Heat-killed bacteria were made by heating at 60°C for 30 min. The culture medium was harvested and used for the incubation with UTnon-FBs.

Statistical analysis

Data are presented as the mean ± SD or SEM. Microsoft Excel and R were used to generate graphs and to perform statistical analyses. P values are indicated as n.s., $P > 0.05$, $*P < 0.05$, and $**P < 0.01$. Data were analyzed by either a two-tailed Student's t test, Fisher's exact test, one-way analysis of variance (ANOVA), or Wilcoxon rank-sum test. The statistical methods used in this study are described in each figure legend. All experiments were performed in triplicate.

Supplementary Materials

This PDF file includes:

Supplementary Materials and Methods

Figs. S1 to S13

Tables S2 to S10

Other Supplementary Material for this manuscript includes the following:

Table S1

Data file S1

MDAR Reproducibility Checklist

[View/request a protocol for this paper from Bio-protocol.](#)**REFERENCES AND NOTES**

- L. C. Giudice, L. C. Kao, Endometriosis. *Lancet* **364**, 1789–1799 (2004).
- L. C. Giudice, Clinical practice. Endometriosis. *N. Engl. J. Med.* **362**, 2389–2398 (2010).
- S. E. Bulun, Endometriosis. *N. Engl. J. Med.* **360**, 268–279 (2009).
- P. Vercellini, P. Viganò, E. Somigliana, L. Fedele, Endometriosis: Pathogenesis and treatment. *Nat. Rev. Endocrinol.* **10**, 261–275 (2014).
- F. L. Cousins, D. F. O., C. E. Gargett, Endometrial stem/progenitor cells and their role in the pathogenesis of endometriosis. *Best Pract. Res. Clin. Obstet. Gynaecol.* **50**, 27–38 (2018).
- R. Kalluri, The biology and function of fibroblasts in cancer. *Nat. Rev. Cancer* **16**, 582–598 (2016).
- L. M. Coussens, Z. Werb, Inflammation and cancer. *Nature* **420**, 860–867 (2002).
- M. B. Buechler, R. N. Pradhan, A. T. Krishnamurthy, C. Cox, A. K. Calviello, A. W. Wang, Y. A. Yang, L. Tam, R. Caothien, M. Roose-Girma, Z. Modrusan, J. R. Arron, R. Bourgon, S. Muller, S. J. Turley, Cross-tissue organization of the fibroblast lineage. *Nature* **593**, 575–579 (2021).
- L. Li, J. M. Miano, P. Cserjesi, E. N. Olson, SM22 alpha, a marker of adult smooth muscle, is expressed in multiple myogenic lineages during embryogenesis. *Circ. Res.* **78**, 188–195 (1996).
- S. J. Assinder, J.-A. Stanton, P. D. Prasad, Transgelin: An actin-binding protein and tumour suppressor. *Int. J. Biochem. Cell Biol.* **41**, 482–486 (2009).
- J. M. Carthy, TGFβ signaling and the control of myofibroblast differentiation: Implications for chronic inflammatory disorders. *J. Cell. Physiol.* **233**, 98–106 (2018).
- E. Tarbit, I. Singh, J. N. Peart, R. B. Rose-Meyer, Biomarkers for the identification of cardiac fibroblast and myofibroblast cells. *Heart Fail. Rev.* **24**, 1–15 (2019).
- M. S. Payne, J. P. Newnham, D. A. Doherty, L. L. Furfaro, N. L. Pental, D. E. Loh, J. A. Keelan, A specific bacterial DNA signature in the vagina of Australian women in midpregnancy predicts high risk of spontaneous preterm birth (the Predict1000 study). *Am. J. Obstet. Gynecol.* **224**, 206.e1–206.e23 (2021).
- K. Agarwal, L. S. Robinson, S. Aggarwal, L. R. Foster, A. Hernandez-Leyva, H. Lin, B. A. Tortelli, V. P. O'Brien, L. Miller, A. L. Kau, H. Reno, N. M. Gilbert, W. G. Lewis, A. L. Lewis, Glycan cross-feeding supports mutualism between Fusobacterium and the vaginal microbiota. *PLOS Biol.* **18**, e3000788 (2020).
- C. A. Brennan, W. S. Garrett, Fusobacterium nucleatum—Symbiont, opportunist and on-cobacterium. *Nat. Rev. Microbiol.* **17**, 156–166 (2019).
- K. N. Khan, A. Fujishita, M. Kitajima, K. Hiraki, M. Nakashima, H. Masuzaki, Intra-uterine microbial colonization and occurrence of endometritis in women with endometriosis. *Hum. Reprod.* **29**, 2446–2456 (2014).
- C. Chen, X. Song, W. Wei, H. Zhong, J. Dai, Z. Lan, F. Li, X. Yu, Q. Feng, Z. Wang, H. Xie, X. Chen, C. Zeng, B. Wen, L. Zeng, H. Du, H. Tang, C. Xu, Y. Xia, H. Xia, H. Yang, J. Wang, J. Wang, L. Madsen, S. Brix, K. Kristiansen, X. Xu, J. Li, R. Wu, H. Jia, The microbiota continuum along the female reproductive tract and its relation to uterine-related diseases. *Nat. Commun.* **8**, 875 (2017).
- S. Crispi, M. T. Piccolo, A. D'Avino, A. Donizetti, R. Viceconte, M. Spyrou, R. A. Calogero, A. Baldi, P. G. Signorile, Transcriptional profiling of endometriosis tissues identifies genes related to organogenesis defects. *J. Cell. Physiol.* **228**, 1927–1934 (2013).
- A. V. Predeus, E. S. Vashukova, A. S. Glotov, M. M. Danilova, N. S. Osinovskaya, O. V. Malysheva, N. Y. Shved, N. Ganbarli, M. I. Yarmolinskaya, T. E. Ivashchenko, V. S. Baranov, Next-generation sequencing of matched ectopic and eutopic endometrium identifies novel endometriosis-related genes. *Russ. J. Genet.* **54**, 1358–1365 (2018).
- A. Hever, R. B. Roth, P. Hevezi, M. E. Marin, J. A. Acosta, H. Acosta, J. Rojas, R. Herrera, D. Grigoriadis, E. White, P. J. Conlon, R. A. Maki, A. Zlotnik, Human endometriosis is associated with plasma cells and overexpression of B lymphocyte stimulator. *Proc. Natl. Acad. Sci. U.S.A.* **104**, 12451–12456 (2007).
- J. Ma, L. Zhang, H. Zhan, Y. Mo, Z. Ren, A. Shao, J. Lin, Single-cell transcriptomic analysis of endometriosis provides insights into fibroblast fates and immune cell heterogeneity. *Cell Biosci.* **11**, 125 (2021).
- R. Liu, M. M. Hossain, X. Chen, J. P. Jin, Mechanoregulation of SM22α/Transgelin. *Biochemistry* **56**, 5526–5538 (2017).
- R. Chakraborty, F. Z. Saddouk, A. C. Carrau, D. S. Krause, D. M. Greif, K. A. Martin, Promoters to study vascular smooth muscle. *Arterioscler. Thromb. Vasc. Biol.* **39**, 603–612 (2019).
- J. Baum, H. S. Duffy, Fibroblasts and myofibroblasts: What are we talking about? *J. Cardiovasc. Pharmacol.* **57**, 376–379 (2011).
- A. Farmawati, Y. Kitajima, T. Nedachi, M. Sato, M. Kanzaki, R. Nagatomi, Characterization of contraction-induced IL-6 up-regulation using contractile C2C12 myotubes. *Endocr. J.* **60**, 137–147 (2013).
- V. J. Young, S. F. Ahmad, W. C. Duncan, A. W. Horne, The role of TGF-β in the pathophysiology of peritoneal endometriosis. *Hum. Reprod. Update* **23**, 548–559 (2017).
- C. O. A. Omwandho, L. Konrad, G. Halis, F. Oehmke, H.-R. Tinneberg, Role of TGF-betas in normal human endometrium and endometriosis. *Hum. Reprod.* **25**, 101–109 (2010).
- S. Chen, M. Kulik, R. J. Lechleider, Smad proteins regulate transcriptional induction of the SM22alpha gene by TGF-beta. *Nucleic Acids Res.* **31**, 1302–1310 (2003).
- G. J. Inman, F. J. Nicolas, J. F. Callahan, J. D. Harling, L. M. Gaster, A. D. Reith, N. J. Laping, C. S. Hill, SB-431542 is a potent and specific inhibitor of transforming growth factor-beta superfamily type I activin receptor-like kinase (ALK) receptors ALK4, ALK5, and ALK7. *Mol. Pharmacol.* **62**, 65–74 (2002).
- R. I. Amann, In situ identification of micro-organisms by whole cell hybridization with rRNA-targeted nucleic acid probes. *Mol. Microb. Ecol. Manual* **3**, 1–15 (1995).
- P. T. Sunde, I. Olsen, U. B. Gobel, D. Theegarten, S. Winter, G. J. Debelian, L. Tronstad, A. Moter, Fluorescence in situ hybridization (FISH) for direct visualization of bacteria in periapical lesions of asymptomatic root-filled teeth. *Microbiology (Reading)* **149**, 1095–1102 (2003).
- T. Thurnheer, R. Gmur, B. Guggenheim, Multiplex FISH analysis of a six-species bacterial biofilm. *J. Microbiol. Methods* **56**, 37–47 (2004).
- L. Karygianni, M. Follo, E. Hellwig, D. Burghard, M. Wolke, A. Anderson, A. Al-Ahmad, Microscope-based imaging platform for large-scale analysis of oral biofilms. *Appl. Environ. Microbiol.* **78**, 8703–8711 (2012).
- K. Bao, N. Bostanci, T. Thurnheer, J. Grossmann, W. E. Wolski, B. Thay, G. N. Belibasakis, J. Oscarsson, Aggregatibacter actinomycetemcomitans H-NS promotes biofilm formation and alters protein dynamics of other species within a polymicrobial oral biofilm. *NPJ Biofilms Microbiomes* **4**, 12 (2018).
- D. Grenier, L. Grignon, Response of human macrophage-like cells to stimulation by Fusobacterium nucleatum ssp. nucleatum lipopolysaccharide. *Oral Microbiol. Immunol.* **21**, 190–196 (2006).
- J. Vallve-Juanico, S. Houshdaran, L. C. Giudice, The endometrial immune environment of women with endometriosis. *Hum. Reprod. Update* **25**, 564–591 (2019).
- M. Benoit, B. Desnues, J.-L. Mege, Macrophage polarization in bacterial infections. *J. Immunol.* **181**, 3733–3739 (2008).
- M. I. Petrova, G. Reid, M. Vanechoutte, S. Lebeer, Lactobacillus iners: Friend or foe? *Trends Microbiol.* **25**, 182–191 (2017).
- J. Ravel, P. Gajer, Z. Abdo, G. M. Schneider, S. S. K. Koenig, S. L. McCulle, S. Karlebach, R. Gorle, J. Russell, C. O. Tacket, R. M. Brotman, C. C. Davis, K. Ault, L. Peralta, L. J. Forney, Vaginal microbiome of reproductive-age women. *Proc. Natl. Acad. Sci. U.S.A.* **108**(suppl. 1), 4680–4687 (2011).
- T. Kato, K. Yasuda, K. Matsushita, K. J. Ishii, S. Hirota, T. Yoshimoto, H. Shibahara, Interleukin-1/-33 signaling pathways as therapeutic targets for endometriosis. *Front. Immunol.* **10**, 2021 (2019).
- H. Liu, R. W. Redline, Y. W. Han, Fusobacterium nucleatum induces fetal death in mice via stimulation of TLR4-mediated placental inflammatory response. *J. Immunol.* **179**, 2501–2508 (2007).
- E. L. V. Haar, J. So, C. Gyamfi-Bannerman, Y. W. Han, Fusobacterium nucleatum and adverse pregnancy outcomes: Epidemiological and mechanistic evidence. *Anaerobe* **50**, 55–59 (2018).
- J. V. Fahey, C. R. Wira, Effect of menstrual status on antibacterial activity and secretory leukocyte protease inhibitor production by human uterine epithelial cells in culture. *J. Infect. Dis.* **185**, 1606–1613 (2002).
- C. R. Wira, M. Rodriguez-Garcia, M. V. Patel, The role of sex hormones in immune protection of the female reproductive tract. *Nat. Rev. Immunol.* **15**, 217–230 (2015).
- A. D. Kostic, E. Chun, L. Robertson, J. N. Glickman, C. A. Gallini, M. Michaud, T. E. Clancy, D. C. Chung, P. Lochhead, G. L. Hold, E. M. El-Omar, D. Brenner, C. S. Fuchs, M. Meyerson, W. S. Garrett, Fusobacterium nucleatum potentiates intestinal tumorigenesis and modulates the tumor-immune microenvironment. *Cell Host Microbe* **14**, 207–215 (2013).
- L. Liu, L. Liang, H. Liang, M. Wang, B. Lu, M. Xue, J. Deng, Y. Chen, Fusobacterium nucleatum aggravates the progression of colitis by regulating M1 macrophage polarization via AKT2 pathway. *Front. Immunol.* **10**, 1324 (2019).

47. L. Ai, Y. Ren, M. Zhu, S. Lu, Y. Qian, Z. Chen, A. Xu, Synbindin restrains proinflammatory macrophage activation against microbiota and mucosal inflammation during colitis. *Gut* **70**, 2261–2272 (2021).
48. Y. W. Han, W. Shi, G. T. Huang, S. K. Haake, N. H. Park, H. Kuramitsu, R. J. Genco, Interactions between periodontal bacteria and human oral epithelial cells: Fusobacterium nucleatum adheres to and invades epithelial cells. *Infect. Immun.* **68**, 3140–3146 (2000).
49. J. Strauss, G. G. Kaplan, P. L. Beck, K. Rioux, R. Panaccione, R. Devinney, T. Lynch, E. Allen-Vercoe, Invasive potential of gut mucosa-derived Fusobacterium nucleatum positively correlates with IBD status of the host. *Inflamm. Bowel Dis.* **17**, 1971–1978 (2011).
50. T. Chen, Q. Li, J. Wu, Y. Wu, W. Peng, H. Li, J. Wang, X. Tang, Y. Peng, X. Fu, Fusobacterium nucleatum promotes M2 polarization of macrophages in the microenvironment of colorectal tumours via a TLR4-dependent mechanism. *Cancer Immunol. Immunother.* **67**, 1635–1646 (2018).
51. H. Li, E. T. Courtois, D. Sengupta, Y. Tan, K. H. Chen, J. J. L. Goh, S. L. Kong, C. Chua, L. K. Hon, W. S. Tan, M. Wong, P. J. Choi, L. J. K. Wee, A. M. Hillmer, I. B. Tan, P. Robson, S. Prabhakar, Reference component analysis of single-cell transcriptomes elucidates cellular heterogeneity in human colorectal tumors. *Nat. Genet.* **49**, 708–718 (2017).
52. S. E. Bulun, B. D. Yilmaz, C. Sison, K. Miyazaki, L. Bernardi, S. Liu, A. Kohlmeier, P. Yin, M. Milad, J. Wei, Endometriosis. *Endocr. Rev.* **40**, 1048–1079 (2019).
53. T. Kurita, Normal and abnormal epithelial differentiation in the female reproductive tract. *Differentiation* **82**, 117–126 (2011).
54. C. Kong, X. Yan, Y. Zhu, H. Zhu, Y. Luo, P. Liu, S. Ferrandon, M. F. Kalady, R. Gao, J. He, F. Yin, X. Qu, J. Zheng, Y. Gao, Q. Wei, Y. Ma, J. Y. Liu, H. Qin, Fusobacterium nucleatum promotes the development of colorectal cancer by activating a cytochrome P450/epoxyoctadecenoic acid axis via TLR4/Keap1/NRF2 signaling. *Cancer Res.* **81**, 4485–4498 (2021).
55. D. A. Morrison, S. A. Lacks, W. R. Guild, J. M. Hageman, Isolation and characterization of three new classes of transformation-deficient mutants of Streptococcus pneumoniae that are defective in DNA transport and genetic recombination. *J. Bacteriol.* **156**, 281–290 (1983).
56. A. D. Greene, S. A. Lang, J. A. Kendzierski, J. M. Sroga-Rios, T. J. Herzog, K. A. Burns, Endometriosis: Where are we and where are we going? *Reproduction* **152**, R63–R78 (2016).
57. S. J. Han, S. Y. Jung, S.-P. Wu, S. M. Hawkins, M. J. Park, S. Kyo, J. Qin, J. P. Lydon, S. Y. Tsai, M.-J. Tsai, F. J. DeMayo, B. W. O'Malley, Estrogen receptor β modulates apoptosis complexes and the inflammasome to drive the pathogenesis of endometriosis. *Cell* **163**, 960–974 (2015).
58. S. J. Han, S. M. Hawkins, K. Begum, S. Y. Jung, E. Kovanci, J. Qin, J. P. Lydon, F. J. DeMayo, B. W. O'Malley, A new isoform of steroid receptor coactivator-1 is crucial for pathogenic progression of endometriosis. *Nat. Med.* **18**, 1102–1111 (2012).
59. Y. Zhao, P. Gong, Y. Chen, J. C. Nwachukwu, S. Srinivasan, C. Ko, M. K. Bagchi, R. N. Taylor, K. S. Korach, K. W. Nettles, J. A. Katzenellenbogen, B. S. Katzenellenbogen, Dual suppression of estrogenic and inflammatory activities for targeting of endometriosis. *Sci. Transl. Med.* **7**, 271ra9 (2015).
60. E. Greaves, F. L. Cousins, A. Murray, A. Esnal-Zufiaurre, A. Fassbender, A. W. Horne, P. T. K. Saunders, A novel mouse model of endometriosis mimics human phenotype and reveals insights into the inflammatory contribution of shed endometrium. *Am. J. Pathol.* **184**, 1930–1939 (2014).
61. S. B. Chadchan, M. Cheng, L. A. Parnell, Y. Yin, A. Schriefer, I. U. Mysorekar, R. Kommagani, Antibiotic therapy with metronidazole reduces endometriosis disease progression in mice: A potential role for gut microbiota. *Hum. Reprod.* **34**, 1106–1116 (2019).
62. J. M. Wessels, M. A. Dominguez, N. A. Leyland, S. K. Agarwal, W. G. Foster, Endometrial microbiota is more diverse in people with endometriosis than symptomatic controls. *Sci. Rep.* **11**, 18877 (2021).
63. K. Akiyama, K. Nishioka, K. N. Khan, Y. Tanaka, T. Mori, T. Nakaya, J. Kitawaki, Molecular detection of microbial colonization in cervical mucus of women with and without endometriosis. *Am. J. Reprod. Immunol.* **82**, e13147 (2019).
64. N. Le, M. Cregger, V. Brown, J. Loret de Mola, P. Bremer, L. Nguyen, K. Groesch, T. Wilson, P. Diaz-Sylvester, A. Braundmeier-Fleming, Association of microbial dynamics with urinary estrogens and estrogen metabolites in patients with endometriosis. *PLOS ONE* **16**, e0261362 (2021).
65. K. N. Khan, A. Fujishita, H. Masumoto, H. Muto, M. Kitajima, H. Masuzaki, J. Kitawaki, Molecular detection of intrauterine microbial colonization in women with endometriosis. *Eur. J. Obstet. Gynecol. Reprod. Biol.* **199**, 69–75 (2016).
66. H. Kajiyama, F. Kikkawa, O. Maeda, T. Suzuki, K. Ino, S. Mizutani, Increased expression of dipeptidyl peptidase IV in human mesothelial cells by malignant ascites from ovarian carcinoma patients. *Oncology* **63**, 158–165 (2002).
67. A. Muraoka, S. Osuka, T. Kiyono, M. Suzuki, A. Yokoi, T. Murase, K. Nishino, K. Niimi, T. Nakamura, M. Goto, H. Kajiyama, Y. Kondo, F. Kikkawa, Establishment and characterization of cell lines from human endometrial epithelial and mesenchymal cells from patients with endometriosis. *F S Sci.* **1**, 195–205 (2020).
68. I. Kawabata, T. Umeda, K. Yamamoto, S. Okabe, Electroporation-mediated gene transfer system applied to cultured CNS neurons. *Neuroreport* **15**, 971–975 (2004).
69. H. Totani, K. Shinjo, M. Suzuki, K. Katsushima, S. Mase, A. Masaki, A. Ito, M. Ri, S. Kusumoto, H. Komatsu, T. Ishida, H. Inagaki, S. Iida, Y. Kondo, Autocrine HGF/c-Met signaling pathway confers aggressiveness in lymph node adult T-cell leukemia/lymphoma. *Oncogene* **39**, 5782–5794 (2020).
70. ENCODE Project Consortium, J. E. Moore, M. J. Purcaro, H. E. Pratt, C. B. Epstein, N. Shores, J. Adrian, T. Kawli, C. A. Davis, A. Dobin, R. Kaul, J. Halow, E. L. Van Nostrand, P. Freese, D. U. Gorkin, Y. Shen, Y. He, M. Mackiewicz, F. Pauli-Behn, B. A. Williams, A. Mortazavi, C. A. Keller, X.-O. Zhang, S. I. Elhajjaj, J. Huey, D. E. Dickel, V. Snetkova, X. Wei, X. Wang, J. C. Rivera-Mulia, J. Rozowsky, J. Zhang, S. B. Chhetri, J. Zhang, A. Victorsen, K. P. White, A. Visel, G. W. Ye, C. B. Burge, E. Lecuyer, D. M. Gilbert, J. Dekker, J. Rinn, E. M. Mendenhall, J. R. Ecker, M. Kellis, R. J. Klein, W. S. Noble, A. Kundaje, R. Guigo, P. J. Farnham, J. M. Cherry, R. M. Myers, B. Ren, B. R. Graveley, M. B. Gerstein, L. A. Pennacchio, M. P. Snyder, B. E. Bernstein, B. Wold, R. C. Hardison, T. R. Gingeras, J. A. Stamatoyannopoulos, Z. Weng, Expanded encyclopaedias of DNA elements in the human and mouse genomes. *Nature* **583**, 699–710 (2020).
71. J. Schindelin, I. Arganda-Carreras, E. Frise, V. Kaynig, M. Longair, T. Pietzsch, S. Preibisch, C. Rueden, S. Saalfeld, B. Schmid, J. Y. Tinevez, D. J. White, V. Hartenstein, K. Eliceiri, P. Tomancak, A. Cardona, Fiji: An open-source platform for biological-image analysis. *Nat. Methods* **9**, 676–682 (2012).
72. Y. Tasaki, M. Suzuki, K. Katsushima, K. Shinjo, K. Iijima, Y. Murofushi, A. Naiki-Ito, K. Hayashi, C. Qiu, A. Takahashi, Y. Tanaka, T. Kawaguchi, M. Sugawara, T. Kataoka, M. Naito, K. Miyata, K. Kataoka, T. Noda, W. Gao, H. Kataoka, S. Takahashi, K. Kimura, Y. Kondo, Cancer-specific targeting of taurine-upregulated gene 1 enhances the effects of chemotherapy in pancreatic cancer. *Cancer Res.* **81**, 1654–1666 (2021).
73. Y. Xue, H. Xiao, S. Guo, B. Xu, Y. Liao, Y. Wu, G. Zhang, Indoleamine 2,3-dioxygenase expression regulates the survival and proliferation of Fusobacterium nucleatum in THP-1-derived macrophages. *Cell Death Dis.* **9**, 355 (2018).

Acknowledgments: We thank the Center for Omics and Bioinformatics, Graduate School of Frontier Sciences, University of Tokyo for the sequencing and its analysis. **Funding:** This work was supported by the Grant-in-Aid for Scientific Research, the Japan Society for the Promotion of Science (19K22674 to A.I., 20H03511 to Y.K., and 20K20598 to Y.K.) and the Research Grant of the Princess Takamatsu Cancer Research Fund (15-24712 to Y.K.). **Author contributions:** Conceptualization: A.M., M.S., and Y.K. Methodology: A.M., M.S., T.H., S.W., K.I., Y.M., K.S., S.O., M.I., T.K., and S.K. Investigation: S.O., Y.H., A.I., H.K., and F.K. Funding acquisition: A.I. and Y.K. Project administration: A.M. and Y.K. Supervision: Y.K. and K.O. Writing—original draft: A.M., M.S., and Y.K. Writing—review and editing: A.M., M.S., and Y.K. **Competing interests:** A patent, Method for detecting bacteria of genus Fusobacterium in order to diagnose endometriosis (WO2023/042714), was submitted (international publication date, 23 March 2023). **Data and materials availability:** The microarray and single-cell data have been deposited in the Genomic Expression Archive (GEA) under accession number E-GEAD-426 and DRA013464, respectively. The 16S sequencing data of the endometrial microenvironment were derived from the European Nucleotide Archive (ENA; <https://ebi.ac.uk/ena/browser/home>) under study numbers PRJEB16013 and PRJEB21098 (17). Bacteria (*F. nucleatum* and *L. iners*) were obtained from the Center for Conservation of Microbial Genetic Resource, Organization for Research and Community Development, Gifu University under a materials transfer agreement (MTA).

Submitted 24 May 2022
Resubmitted 07 November 2022
Accepted 24 May 2023
Published 14 June 2023
10.1126/scitranslmed.add1531